Nuclear Science

NEA/NSC/DOC(2004)7
ISBN 92-64-02072-1

Benchmark on Beam Interruptions in an Accelerator-driven System

Final Report on Phase II Calculations

A. D'Angelo
ENEA/Casaccia (Italy)

B. Arien, V. Sobolev, G. Van den Eynde
SCK•CEN (Belgium)

F. Gabrielli
Politecnico di Torino, Dipartimento di Energetica (Italy)

NEA No. 5422

NUCLEAR ENERGY AGENCY
ORGANISATION FOR ECONOMIC CO-OPERATION AND DEVELOPMENT

ORGANISATION FOR ECONOMIC CO-OPERATION AND DEVELOPMENT

Pursuant to Article 1 of the Convention signed in Paris on 14th December 1960, and which came into force on 30th September 1961, the Organisation for Economic Co-operation and Development (OECD) shall promote policies designed:

- to achieve the highest sustainable economic growth and employment and a rising standard of living in member countries, while maintaining financial stability, and thus to contribute to the development of the world economy;
- to contribute to sound economic expansion in member as well as non-member countries in the process of economic development; and
- to contribute to the expansion of world trade on a multilateral, non-discriminatory basis in accordance with international obligations.

The original member countries of the OECD are Austria, Belgium, Canada, Denmark, France, Germany, Greece, Iceland, Ireland, Italy, Luxembourg, the Netherlands, Norway, Portugal, Spain, Sweden, Switzerland, Turkey, the United Kingdom and the United States. The following countries became members subsequently through accession at the dates indicated hereafter: Japan (28th April 1964), Finland (28th January 1969), Australia (7th June 1971), New Zealand (29th May 1973), Mexico (18th May 1994), the Czech Republic (21st December 1995), Hungary (7th May 1996), Poland (22nd November 1996), Korea (12th December 1996) and the Slovak Republic (14 December 2000). The Commission of the European Communities takes part in the work of the OECD (Article 13 of the OECD Convention).

NUCLEAR ENERGY AGENCY

The OECD Nuclear Energy Agency (NEA) was established on 1st February 1958 under the name of the OEEC European Nuclear Energy Agency. It received its present designation on 20th April 1972, when Japan became its first non-European full member. NEA membership today consists of 28 OECD member countries: Australia, Austria, Belgium, Canada, the Czech Republic, Denmark, Finland, France, Germany, Greece, Hungary, Iceland, Ireland, Italy, Japan, Luxembourg, Mexico, the Netherlands, Norway, Portugal, Republic of Korea, the Slovak Republic, Spain, Sweden, Switzerland, Turkey, the United Kingdom and the United States. The Commission of the European Communities also takes part in the work of the Agency.

The mission of the NEA is:

- to assist its member countries in maintaining and further developing, through international co-operation, the scientific, technological and legal bases required for a safe, environmentally friendly and economical use of nuclear energy for peaceful purposes, as well as
- to provide authoritative assessments and to forge common understandings on key issues, as input to government decisions on nuclear energy policy and to broader OECD policy analyses in areas such as energy and sustainable development.

Specific areas of competence of the NEA include safety and regulation of nuclear activities, radioactive waste management, radiological protection, nuclear science, economic and technical analyses of the nuclear fuel cycle, nuclear law and liability, and public information. The NEA Data Bank provides nuclear data and computer program services for participating countries.

In these and related tasks, the NEA works in close collaboration with the International Atomic Energy Agency in Vienna, with which it has a Co-operation Agreement, as well as with other international organisations in the nuclear field.

FOREWORD

Recognising the need to evaluate thermal responses of accelerator-driven systems to a beam trip, the OECD/NEA Working Party on Scientific Issues in Partitioning and Transmutation (WPPT) is organising a series of benchmarks on beam interruptions in lead-bismuth-cooled and MOX-fuelled accelerator-driven systems. The series will range from the simple to the complex.

The first phase of the benchmarks evaluated temperature and power variations induced by beam interruptions of different durations with models of minimal phenomenological and computational complexity. The first phase was completed in 2003. The present phase of the benchmarks (Phase II) was designed to investigate temperature variations under fresh fuel conditions for four different fuel power density cases and two interruption durations.

This report summarises the comparative analysis of the ten sets of fuel and coolant temperature variation results provided. In addition, a comprehensive analysis was carried out of sensitivities to models and data assumed in the calculations.

In order to investigate more complex calculation assumptions and computational methods, a subsequent phase of the benchmarks is being defined, which may be extended to cover irradiated fuel conditions.

Acknowledgements

The Secretariat expresses its sincere gratitude to the participants who were willing to devote their time and effort to this benchmark exercise.

Abstract

Temperature transients induced by beam interruptions of different duration in a lead-bismuth-cooled and MOX-fuelled experimental ADS are investigated as a computational benchmark problem. This second phase of calculations aims to investigate the impact on the transient results and uncertainties of different fuel power density conditions. Temperature variations are investigated assuming fresh fuel conditions, four different fuel power densities and two interruption durations. The results provided by the nine participants are presented and compared in this final report. In addition, uncertainty components due to the different assumptions on model and data recommended in the benchmark specification is evaluated by means of the sensitivity studies carried out by some participants as supplementary contributions.

TABLE OF CONTENTS

Chapter 1
INTRODUCTION

The results of the second phase of benchmark calculations relevant to beam interruptions in a lead-bismuth cooled and MOX-fuelled accelerator-driven system (ADS) are presented, compared and analysed in this final report. It is worth briefly mentioning that the first phase of calculations [1], mainly devoted to the comparative assessment of the different computation methods, was a success in that the results obtained using different codes agreed within about 3%. This second phase of calculations mainly aims to investigate the transient results and their uncertainties under different fuel power density conditions. To this aim, the proposed transient calculations are not only relevant to an XADS-type average fuel pin, but also to the case of the XADS-type hottest fuel pin and to the average and hottest pin cases of the MYRRHA-type experimental ADS. The benchmark specification is provided as Appendix I of this report. Practically, the benchmark participants calculate four sets of beam interruption solutions, called "reference results", by assuming models and data recommended in the benchmark specification for the following four cases:

A) ANSALDO-XADS system-type average fuel pin (~80 W/cm);

B) ANSALDO-XADS system-type hottest fuel pin (~115 W/cm);

C) MYRRHA-XADS system-type average fuel pin (~220 W/cm);

D) MYRRHA-XADS system-type hottest fuel pin (~320 W/cm).

Moreover, to evaluate the uncertainty of the results, the benchmark calculations have also been extended to "sensitivity analyses" as regards assumptions (on models and data) different from those recommended in the benchmark specification. The participants also evaluate the impact of any assumption they thought to be a valid alternative or an improvement upon the recommendations given in the benchmark specification. As in the first phase of calculations, some simplifications have been assumed to have a minimum impact on the temperature variations either in the ANSALDO-type or in the MYRRHA-type XADS loaded with fresh fuel. This was done so that the benchmark results presented in this final report would allow to evaluate, under BOL fuel conditions, the average and hottest pin initial temperature distributions, temperature variations induced by accelerator beam interruptions having different durations and corresponding uncertainties.

Concerning the structure of this final report, Chapter 2 is devoted to the participants and a list of the codes used. Chapter 3 compares the "reference results" obtained by the different participants. For each of the four fuel power density values considered (Cases A to D), the dispersion of the temperature results calculated by the different participant is evaluated. More in detail, the first part of this chapter is devoted to the results of initial steady-state axial temperature distributions (common to all the considered beam interruption transients):

- the fuel centreline temperature;
- the fuel surface temperature;

- the clad surface temperature;
- the coolant temperature.

Also reported in Chapter 3 are the time-depending results of:

- fuel centreline temperature at the fuel zone mid-plane;
- outlet coolant temperature.

Time-depending results concern the four fuel power density values considered and both the 1 s and the 6 s beam interruptions. A synthesis of the outlet coolant temperature sensitivity analyses performed by different participants is also provided in order to explain why outlet coolant temperatures are particularly precise, independent of the fuel power density conditions.

Chapter 4 is devoted to the results concerning the sensitivity analysis of both the steady-state and transient fuel temperatures. Namely, the impact on reference results (Cases A to D) of assumptions (on models and data) that the participants thought to be a valid alternative or an improvement compared to the recommendations given in the benchmark specification is reported. The aim of this investigation is to evaluate the reference result uncertainties following the benchmark recommendations on models and data. The general coherence of the different benchmark results is the subject of Chapter 5. Some concluding remarks close the present final report (Chapter 6).

Chapter 2

BENCHMARK PARTICIPANTS AND CODES USED

Table 1 reports the names of the nine participants of this second phase of benchmark calculations and the codes they used. Due to the fact that PSI solved the benchmark problems using two different calculation tools, there are a total of ten sets of contributions.

Table 1. Participant and code list

Participant	*From*	*Code used*
Antonio D'Angelo F. Gabrielli	ENEA Casaccia (Italy)	TIESTE-MINOSSE
Gert Van den Eynde Baudouin Arien	SCK•CEN Mol (Belgium)	SITHER-PKS
Kazafumi Tsujimoto	JAERI Tokai (Japan)	EXCURS-M
Marcus Eriksson	Royal Institute of Technology Stockholm (Sweden)	SASSYS/SAS4A
Michael Schikorr	FZK Karlsruhe (Germany)	SIM-ADS
Paul Coddington Konstantin Mikityuk_1	PSI (Switzerland)	TRAC-M/AAA
Paul Coddington Konstantin Mikityuk_2	PSI (Switzerland)	LOOP2
Pieter Wakker Jim Kuijper	NRG Petten/Arnhem (The Netherlands)	TRAC MOD
Ron Dagan Cornelis Broeders	FZK Karlsruhe (Germany)	SAS4-ADS
Yonghee Kim	KAERI Daejeon (Republic of Korea)	DESINUR

It is worthwhile to reiterate that the specification of this benchmark second phase concerns single fuel channel thermal-hydraulics coupled with a point kinetics model of average and hottest fuel pins relevant to two lead-bismuth-cooled and MOX-fuelled XADS (the four cases previously designated A, B, C and D). In particular, the model refers to the "fresh fuel" assumption corresponding to the BOL fuel condition. Irradiated fuel conditions are foreseen to be investigated in the near future.

Chapter 3

REFERENCE RESULTS

As mentioned earlier, the “reference results” are obtained by the participants by assuming models and data as close as possible to those recommended in the benchmark specification. The definition of models and data recommended in the specification is complete, meaning that in principle the benchmark problem should have not any degree of freedom and that only the numerical solution of the same equations could induce differences in the participant solutions. In reality, this is not precisely the case; different codes can often be only forced by the users to adopt models and data as close as possible to those recommended in the benchmark specification. The calculation results of the first phase of benchmark demonstrated that the effect of different codes (i.e. also of slightly different assumptions) to calculate temperature transients induced by beam interruptions of different duration is not significant in the case of the calculations relevant to Case A (ANSALDO XADS average pin), characterised by a low fuel power density level. The present second phase of calculations aims to extend the reference result for an investigation to higher values of fuel power density. For the sake of completeness it should be noted that the specification of the current Case A of this second phase of calculations is just slightly different from that of the first phase. In fact, in order to satisfy a participant request for this second phase of calculations, a saturated decay heat level (6% of the total power) at the beginning of any considered beam interruption has been assumed (instead of no-decay heat power).

Initial steady-state axial temperature distributions

Figures 1-4 show the ten sets of steady-state axial temperature distributions calculated by participants for Cases A to D, respectively. In these figures, the highest temperature set is relevant to the fuel centreline axial distribution. Results relevant to the fuel surface temperature, the clad surface temperature and the coolant temperature are drawn at progressively lower temperatures in the same figures. As expected, higher fuel power density cases are characterised by higher fuel temperatures. Specifically, from Case A to Case D, the fuel temperature at the fuel zone mid-plane increases from about 1 000 K to about 2 300 K. Moreover, despite the general agreement on temperature results, larger relative dispersions of the fuel temperatures calculated by the different participants look evident for higher fuel power levels (i.e. for higher heat fluxes through the fuel pin materials and interfaces). In particular, as evidenced in Figures 1-4, the relative dispersion of the temperatures calculated by different participants (in Kelvin degrees at fuel mid-plane) increases from Case A to D, from the quite insignificant 1.8% value to 3.0%, 5.0% and 5.6% respectively. This trend of growing dispersions will be recalled in the next chapter and discussed along with sensitivities to models and data assumed in the calculations.

Transient (time-depending) results

Fuel temperatures

Figures 5-8 show the ten sets of time-depending results relevant to the fuel centreline temperature at the fuel zone mid-plane calculated by participants for the Cases A to D. As expected, the reduction

of the fuel centreline temperature (just before the beam recovery) induced by the beam interruptions depend on the case considered. For instance (and as also reported in Tables 1-3), the fuel centreline temperature variation induced by beam interruptions belonging 1 s increases from 60÷65 K in Case A to about 90, 190 and 260 K in cases B through D.

The relative dispersions among the fuel temperatures (K) obtained by the different participants look to be largely independent of the time in both the considered (1 s and 6 s) beam interruptions. For this reason, the relative dispersion of the temperature variations also remains of the same order of magnitude during the whole transient; the relative dispersion of the fuel centreline temperature results increases (roughly, by a factor 2) going from XADS-type to MYRRHA-type cases. Moreover, it looks to remain close to the 1.8%, 3.0%, 5.0% and 5.6% values mentioned above for the steady-state (initial) condition (from Case A to D). This consideration is clearly significant in simplifying the result uncertainties and will be confirmed by the sensitivity study of fuel temperature results as regards models and data assumed in the calculations (see Chapter 4).

Outlet coolant temperatures

Figures 9-12 show the ten sets of results relevant to the outlet coolant temperature transients induced by beam interruptions of 1 s or 6 s, for Cases A to D. It appears evident that both the steady-state and the transient coolant temperature results are particularly precise. They do not show significant dispersions in either case. The low dispersions look to be independent of the fuel power density: i.e. roughly the same (1%) in the four cases considered. This is confirmed by the sensitivity study of outlet coolant results as concerns models and data assumed in calculations.

Outlet coolant temperature variations induced by beam interruptions in XADS are of interest regarding the evaluation of possible thermal stresses to the core structure and to the intermediate heat exchangers. The outlet coolant temperature reduction induced by beam interruptions of 6 s goes from about 60 K in Case A to about 80, 90 and 140 K in Cases B, C and D, as is also reported in Tables 2-4.

Contrary to what has previously discussed with regard to fuel temperatures, calculated coolant temperatures continuously appear to be very precise. Steady-state and transient coolant temperature results determined by the different participants do not show significant relative dispersions (about 1% only) in all the ANSALDO and MYRRHA XADS cases considered.

The sensitivity analyses performed by some participants confirm that the coolant temperature results are particularly precise. All the investigated variations of calculation assumptions lead to negligible or relatively limited effects on the calculated coolant temperatures: no more than 3% (20 K/670 K) for a variation of 10% in the coolant specific heat (SCK•CEN investigation). Practically, this signifies negligible effects of slightly different assumptions on models or data that the participants made unintentionally when utilising their codes for reference calculations.

Chapter 4

FUEL TEMPERATURE SENSITIVITY RESULTS

A) PDS-XADS-type average fuel pin

The sensitivities of fuel temperature results to the recommendations given in the benchmark specification on models and data can be significant. Moreover, fuel temperature sensitivities calculated by the participants seem to increase when higher fuel power density cases are considered (i.e. when higher heat fluxes through the fuel pin materials and interfaces are considered). The benchmark specification (see Appendix I) stressed the opportunity for participants to concentrate a larger effort toward sensitivity studies (in the way of optional contributions), pointing out the most significant perturbations of calculation assumptions (possibly, having impacts larger than 5%). For this reason, the benchmark participants investigated more the sensitivities of the results obtained in Case D than those obtained in cases characterised by lower fuel power densities.

MOX fuel thermal-conductivity

Figure 13 shows two sensitivity studies, performed by FZK (SAS4-ADS code) and by ENEA (TIESTE-MINOSSE code), on the impact of different assumptions to calculate the fuel centreline temperatures under steady-state conditions. The ENEA study concerns only the fuel temperature relative variation due to the use of a different MOX fuel thermal conductivity evaluation. Specifically, ENEA tested the impact on Case A fuel temperatures of assuming the MOX fuel conductivity recommended in the benchmark specification to calculate the Cases C and D. Figure 14 shows the low dependence on time of sensitivities during the transient induced by a 1 s beam interruption. Steady-state fuel temperatures (K), time-depending fuel temperatures (K) and fuel temperature variations in comparison with the (steady) initial condition have similar sensitivities (and therefore have similar uncertainties).

The MOX fuel thermal conductivity recommended by SCK•CEN in the MYRRHA cases (see Annex II of the Phase II benchmark specification) comes from Daniel Baron's evaluation [2]. Figure 15 shows that this MOX fuel thermal conductivity is about 0.6 W/(m K) lower at T < 1 800 K than that recommended by the ENEA in the PDS-XADS cases. In Ref. [3], Daniel Baron evaluates the standard deviation of experimental data on the UO_2, PuO_2 and MOX fuel thermal conductivity to be of the same order [about 0.6 W/(m K)]. Therefore, the value of about 2% evaluated by the ENEA as the impact of the assumption of the Baron's MOX fuel thermal conductivity is also the fuel temperature uncertainty due to the uncertainty of the fuel thermal conductivity data. Moreover, Daniel Baron designates as a "central prediction" his fuel thermal conductivity formulation (close to the formulation recommended by the SCK•CEN). Finally, by considering both the standard deviation and the probable systematic in comparison with the central values, the uncertainty for the PDS-XADS-type average fuel temperatures (K) and temperature variations can be evaluated to be about 3%.

Fuel-to-clad-gap model

The fuel-to-clad-gap model recommended for the PDS-XADS-type is very simple but also particularly conservative: the gap thickness is assumed to be temperature independent but always equal to the thickness at room temperature. Below, it will be shown that, due to the low PDS-XADS fuel power density, the fuel temperature overestimation induced by this (simple) model can be accepted because it remains lower than 2.5% even in the case of the hottest pin. No uncertainty contribution will be associated to the PDS-XADS reference calculations for this model assumption that resulted to be significantly conservative.

The about 6% larger temperature impact calculated by FZK (Ron Dagan and Cornelis Broeders) using a particular model and data option of the SAS4ADS code (reported in Figure 13) is compatible with the 3% uncertainty [one standard deviation (s.d.)] due to the MOX fuel thermal conductivity.

Total uncertainty of the calculated fuel temperatures

The uncertainty due to the fuel thermal conductivity recommendation is the only significant component resulting in the case of the PDS-XADS average pin calculations. Thus, a total uncertainty of about 3% (at one s.d.) can be evaluated for the PDS-XADS average-pin fuel temperature (K) and temperature variations induced by beam interruptions and calculated by assuming the benchmark recommendations.

B) PDS-XADS-type hottest fuel pin

Figure 16 shows four sensitivity studies, by SCK•CEN (SITHER-PKS code) and by ENEA (TIESTE-MINOSSE code), concerning different assumptions in the calculation of the fuel centreline temperature distributions relevant to the PDS-XADS-type hottest fuel pin (Case B).

MOX fuel thermal-conductivity

Two studies concern the fuel temperature relative variation due to the use of a different MOX fuel thermal conductivity evaluation. Namely, SCK•CEN evaluated the impact on fuel temperatures of a MOX fuel conductivity 10% lower than that recommended. ENEA evaluated the impact of assuming the [about 0.6 W/(m K) lower] MOX fuel conductivity recommended in the benchmark specification for the MYRRHA cases. Considering that different reductions of the fuel thermal conductivities (10% or about 15%) have been investigated, the sensitivity leading to the two effects on the fuel temperatures can be well determined. Both results indicate that Baron's MOX fuel thermal conductivity increases the fuel temperature by about 3% in the hottest pin mid-plane.

Moreover, we can (also in this case) say that the resulting 3% of fuel temperature variation (increasing) is of the same order of magnitude of the (one standard deviation) uncertainty due to the (uncertainty on the) fuel thermal conductivity data themselves. Finally, by considering both the standard deviation and the probable systematic in comparison with Baron's central values, an uncertainty of 4÷5% can be evaluated for the PDS-XADS-type hottest fuel temperatures.

Figure 17 shows a low dependence on time of sensitivities during the transient induced by a 1 s beam interruption (as in the previous Case A).

Clad-coolant heat exchange model

Figure 16 also shows the SCK•CEN result concerning the impact on fuel temperatures of a different assumption on the clad-coolant heat exchange model. The clad-coolant heat exchange correlation recommended for the MYRRHA calculations would lead to slightly lower PDS-XADS fuel temperatures (within about 1%). No uncertainty contribution will be associated with the model assumption on the clad-coolant heat exchange.

Fuel-to-clad-gap model

Figure 16 also displays the SCK•CEN result concerning the impact of the temperature-depending gap thickness model (recommended for the MYRRHA cases) instead of the constant (room temperature) thickness simplified model recommended for the PDS-XADS calculations. The temperature-depending gap thickness model would lead to slightly lower fuel temperatures (less than 2.5%). No uncertainty contribution will be associated with the PDS-XADS reference calculations for this significantly conservative model assumption.

Total uncertainty of the calculated fuel temperatures

The uncertainty due to the fuel thermal conductivity recommendation is the only significant uncertainty component that can be evaluated in the case of the PDS-XADS average pin calculations. Therefore, a total uncertainty of about 4.5% (at one s.d.) can be evaluated for the PDS-XADS hottest-pin fuel temperature (K), and temperature variations induced by beam interruptions.

C) MYRRHA-type average fuel pin

Figure 18 shows five sensitivity studies on the impact of different assumptions to calculate the fuel centreline temperature steady-state values relevant to the MYRRHA-type average fuel pin (Case C). Four were performed by the ENEA (TIESTE-MINOSSE code) and one by FZK (SIM-ADS code).

MOX fuel thermal-conductivity

As concerns the impact of the recommended fuel thermal conductivity on the MYRRHA average fuel temperature calculation for the XADS cases, the excellent agreement between the ENEA and FZK results is evident. The use of the ENEA recommendation would lead to about 6% lower fuel temperatures at the mid-plane of the MYRRHA average pin. As for the previous Cases A and B, Figure 19 shows the relatively low dependence on time of the fuel temperature sensitivities during a transient induced by a 1 s beam interruption. Again, this means that steady-state fuel temperatures (K), time-depending fuel temperatures (K) for 1 s beam interruptions and fuel temperature variations with respect to the (steady) initial condition have similar sensitivities (and therefore similar uncertainties).

As previously mentioned, Daniel Baron designates as a “central prediction” his fuel thermal conductivity formulation (which is close to that recommended by SCK•CEN) [3]. Moreover, he evaluates the standard deviation of this central evaluation to be of the same order of magnitude [about 0.6 W/(m K)] of the difference between the ENEA and the SCK•CEN recommendations. Finally, the roughly 6% fuel temperature variation calculated by the ENEA and FZK is of the same order of magnitude of the fuel temperature uncertainty induced by data on the fuel thermal conductivity.

Fuel-to-clad-gap model

Figure 18 also shows the ENEA results concerning the impact of assuming constant thickness (at room temperature) gap conductivity. It is evident that, in the MYRRHA conditions, this simplified model would lead to too-high temperature evaluations. Specifically, the simplified model induces a pin fuel temperature overestimation of about 10% at the fuel zone mid-plane. The temperature-depending gap thickness assumption recommended by SCK•CEN is thus confirmed to be opportune for MYRRHA cases. Figure 18 further displays the results of an ENEA investigation on the uncertainty associated with the temperature-depending gap thickness model. ENEA investigated the maximum uncertainty induced by the degree of freedom relevant to the definition of a "mean" fuel temperature; that is, the fuel temperature recommended to evaluate the fuel linear expansion (strain) during the transients. As an extreme case, the ENEA calculated the impact of considering the same fuel linear expansion as a function of the fuel surface temperature. Figure 18 shows that this choice could induce significant fuel temperature variations. An uncertainty of about 3% can be conservatively retained as associated with this degree of freedom in choosing the temperature which drives the fuel surface expansion during transients.

Clad-coolant heat exchange model

Also demonstrated in Figure 18 is the lack of significance of the impact on fuel temperatures of a different assumption on the clad-coolant heat exchange model (the impact evaluation is within 2%).

As in the previous cases, Figure 19 shows the low dependence on time of the investigated sensitivities during a transient induced by a 1 s beam interruption.

Total uncertainty of the calculated fuel temperatures

Combining the 6% and 3% uncertainty components (one s.d.), previously evaluated as effects of the fuel thermal conductivity and the gap model respectively, a total uncertainty of about 7% is established with regard to the MYRRHA average-pin fuel temperature (K) and temperature variations induced by beam interruptions.

D) MYRRHA-type hottest fuel pin

Figure 20 shows a large number of sensitivity studies carried out by ENEA (TIESTE-MINOSSE code), SCK•CEN (SITHER-PKS code), PSI (LOOP2 code) and by FZK (SIM-ADS code). Figure 21 shows the low time dependence of the investigated sensitivities (as in the previous cases). This figure also includes some additional sensitivity studies, for example the investigation on the impact of the fuel axial expansion undertaken by the Royal Institute of Technology, Stockholm-Sweden (SASSYS/ SAS4A code).

MOX fuel thermal-conductivity

Figure 20 shows an excellent agreement between ENEA, FZK and SCK•CEN results concerning the impact of the fuel thermal conductivity recommended for the XADS cases. As discussed above for Case C, we can say that the approximately 6% fuel temperature variation calculated by ENEA and FZK that results from using the ENEA-recommended fuel thermal conductivity is of the same order of magnitude of the uncertainty on the fuel thermal conductivity.

Clad-coolant heat exchange model

Figure 20 shows a very good agreement between the ENEA and the SCK•CEN sensitivity study concerning the clad-coolant heat exchange correlation. The use of the correlation assumed for PDS-XADS cases led to only slightly more elevated fuel temperatures (within about 2%). One per cent (1%) of one s.d. uncertainty will be taken into account for the slightly non-conservative model on the clad-coolant heat exchange used in the MYRRHA calculations.

Fuel-to-clad-gap model

Concerning a possible approximation by the constant thickness (at room temperature) gap conductivity model (recommended for the PDS-XADS cases), Figure 20 shows two impact evaluations, one by the ENEA and one by SCK•CEN. Also in this case it appears evident that the simplified model leads to temperature evaluations under the MYRRHA conditions of higher fuel power densities that are largely too conservative. The agreement on the corresponding fuel temperature increase is worse than for the other evaluations. Nevertheless, both evaluations reconfirm the usefulness of the temperature-depending gap thickness assumption in the MYRRHA heat flux conditions. Figure 20 also displays results for an ENEA investigation concerning the uncertainty associated with this temperature-depending gap thickness model. As in the previous MYRRHA average case, ENEA tested the uncertainty induced by the definition of an extreme fuel temperature to evaluate the fuel surface linear expansion (strain) during the transients. Also in this case, the ENEA calculated the impact of assuming the fuel surface temperature to be driving the linear expansion. Figure 20 shows that this extreme choice induces a fuel temperature increase that may be significant. An uncertainty of 4% (one s.d.) can be conservatively retained for the degree of freedom in choosing the temperature driving the fuel surface expansion during a transient.

Figures 20 and 21 show the results of a further sensitivity study performed by PSI on the fuel and clad (internal) surface roughness impact on the gap thickness evaluation. Namely, the following Ross and Stoute model [4,5] for the α_g gap conductance was assumed in the LOOP2 code calculation:

$$\alpha_g = \frac{\lambda_g}{\Delta_g + C(\rho_f + \rho_c) + (g_f + g_c)} + \alpha_{rad}$$

where λ_g is the thermal conductivity of gas composition, Δ_g is the fuel-clad gap radial thickness, C is the empirical constant (C = 3.2), ρ_f and ρ_c are the fuel and clad surface roughness, g_f and g_c are the temperature jump distances, and α_{rad} is the radiation component.

The roughness terms increase the effective gap thickness. The temperature jump distance terms account for the non-linear gas temperature variation near the fuel and cladding surfaces.

If the gas gap is filled with pure helium then [2]:

$$g_1 + g_2 = 0.024688\ \lambda_g\ T^{1/2} / (p_g a_{He} M^{-1/2})$$

where T and p_g are the gap gas temperature and pressure, M is the molecular weight of helium and $a_{He} = 0.425\text{-}2.3\cdot10^{-4}T$ is the accommodation coefficient for helium.

PSI assumes (pessimistically) a two-micron roughness for both the fuel and the clad surfaces ($\rho_f = \rho_c = 2\ \mu$). The Ross and Stoute model provides an extra thickness of the gap corresponding to 12.8 microns for roughness and 3.46 microns for temperature jumps. It is evident that the dominant

correction is the correction due to the roughness. The total 16.3 microns of extra thickness (25% of the about 66 micron gap dimension at t = 0) can lead to the variation of about 2.8% on the initial fuel centreline temperature at the core mid-plane (Figure 20 steady-state evaluation).

Finally, in the case of MYRRHA hottest, a 2% uncertainty can be conservatively retained as contributing to the fuel–gap internal surface roughness, not defined in the benchmark specification.

MOX fuel specific heat

The uncertainty of the UO_2 specific heat can be evaluated as equal to 0.7% up to 2 000 K and to 6% from 2 000 K to melting point [6]. For the PuO_2 specific heat, the uncertainty can be evaluated as equal to 2% from 298 K up to 1 800 K and to 13% from 1 800 K to melting point [7]. Practically, the uncertainty of the (20.5% PuO_2) MOX fuel specific heat is only 1% below 1 800 K, but increases to about 7.5% above 2 000 K. In the case of the MYRRHA hottest fuel pin, this important increase of uncertainty above 1 800 K can induce a significant uncertainty component. If it is conservatively evaluated that the hottest fuel pin temperatures can be higher than 1 800 ÷ 2 000 K in 25% of its fuel volume, an average uncertainty of about 3% can be conservatively associated with the corresponding heat capacity.

The fuel specific heat has no impact on the initial (steady-state) fuel temperatures, but only on fuel temperatures during the transient. This means that, as a peculiarity of this parameter, specific heat can easily induce significant effects on the calculated values of the fuel temperature decrease induced by beam interruptions. Figure 22 shows the specific heat effect on the fuel temperature variation from its initial value (obtained using the impact evaluated by SCK•CEN on the fuel temperature absolute value). Practically, a 10% lower fuel specific heat can induce about 9% larger fuel temperature decrease induced by a 1s beam interruption. Therefore, the about 3% uncertainty (one s.d.) of the MYRRHA hottest fuel specific heat can lead to about a 2.7% uncertainty component on the fuel temperature decrease induced by beam interruptions.

Fuel (axial) and core structure (radial) expansions

The impact on fuel temperatures of models for determining the reactivity feedback from axial fuel expansion/contraction and radial core structural expansion/contraction has been investigated by the Royal Institute of Technology, Stockholm-Sweden (SASSYS/SAS4A code). The assumed reactivity coefficients were based on a typical MOX-fuelled LMR:

Axial expansion (free fuel)	-0.41 pcm/K
Radial expansion	-0.68 pcm/K

The fuel and core motions were based solely on their thermal expansion. The axial fuel expansion model uses a fuel reactivity worth curve to compute the reactivity changes by assuming that the reactivity contributions of the different nodes are proportional to the local mass changes. The fuel was assumed to expand freely in the jacket. The core radial expansion model combines the grid plate expansion effect and subassembly bowing reactivity into one equation that describes the reactivity as proportional to the change in inlet temperature and in the above-core load pad temperature.

The main reason for deviation from the reference results shown in Figure 23 is due to the reactivity contribution from axial fuel expansion. The impact is not significant for the 1 s interval interruption. Even for the 6 s interval interruption case, the impact on fuel temperature (K) becomes significant

only after the beam recovery, i.e. (as expected for a feedback effect) when a fuel temperature increase occurs. Therefore, even this most significant effect occurs when the fuel temperature is unimportant for calculating either the fuel temperature minimum values or the fuel temperature maximum decrease (of interest for possible thermal stresses induced by beam interruptions).

Finally, this sensitivity analysis seems to confirm one of the calculation conclusions from Phase I: the main benchmark results, and in particular the temperature variations induced by beam interruptions, are largely independent of feedback effects. The present benchmark specification concerns beam interruptions which occur under operational conditions, i.e. characterised by a large subcriticality (about -8$). A greater importance of neutron kinetics would be expected under less subcritical conditions. For the XADS systems investigated, however, the lower subcriticality can not occur under operational conditions.

Total uncertainty of the calculated fuel temperatures

Combining the 6%, 1%, 4%, 2% and 2.7% components conservatively evaluated as effects of the fuel thermal conductivity, the clad-coolant heat exchange model, the gap model, the Ross-Stoute gap-extra-width and the fuel heat capacity uncertainties respectively, 8% of total uncertainty can be evaluated for the MYRRHA hottest-pin fuel temperature variations induced by 1 s beam interruptions. In principle, due to the lack of the uncertainty component relevant to the heat capacity, the uncertainty of both the initial and the asymptotic absolute temperatures (K) would be just slightly lower (about 7.5% at one s.d.). Moreover, the uncertainty for the Ross-Stoute gap-extra-width will be solved in the future by defining the gap surface roughness conditions. But for the sake of simplicity, 8% uncertainty can be assumed at present and can be conservatively extended to the absolute fuel temperatures.

Chapter 5

GENERAL COHERENCE OF THE BENCHMARK DIFFERENT RESULTS

The sensitivity analysis clearly points out that the outlet coolant temperature results are independent of the calculation assumptions. This consideration appears coherent with the very precise outlet coolant temperature "reference results" obtained by the different participants using different codes: always within about 1%, independent of the fuel power density condition relevant to the four cases considered.

On the other hand, the fuel temperatures are clearly dependent on some calculation assumptions. In particular, calculated fuel temperature depends mainly on the fuel thermal conductivity data and the fuel-to-clad heat transfer model. The corresponding sensitivities increase for larger fuel power density cases. Consequently, the uncertainties of the fuel temperatures (K) and of their variations also increase for larger fuel power density cases: 3%, 4.5%, 7% and 8% going from Case A to Case D.

This sensitivity trend also appears to be coherent with the dispersion of the "reference results" concerning the fuel temperatures, which clearly increase for larger fuel power density cases: 1.8%, 3%, 5% and 5.6% going from Case A to Case D. This coherence seems to indicate that the dispersions of the reference results are only due to the effects of slightly different assumptions on models or data that the participants made unintentionally, although they have tried to reproduce as well as possible the benchmark recommendation.

Chapter 6

CONCLUDING REMARKS

Beam interruptions were investigated in the framework of the second phase of OECD/NEA/WPPT computational benchmark calculations. Two lead-bismuth-cooled and MOX-fuelled experimental accelerator-driven systems, characterised by two different fuel power densities, were considered: the PDS and the MYRRHA XADS. Initial temperatures and transients induced by beam interruptions of different duration were calculated either for the average or for the hottest fuel pin case. The 10 sets of coolant and fuel temperature results, calculated by the nine participants, were compared and the corresponding dispersions were evaluated. This second phase of benchmark calculations was also aimed to analyse the sensitivities to models and data assumed in the calculations. To this aim, the benchmark has been successful: sensitivities calculated by different participants were compared and used to evaluate the reference result uncertainties. Resulting temperature variations induced by 1 s or 6 s beam interruptions are reported in Tables 1-4, along with their uncertainties. Finally, the general coherence among reference result dispersions and sensitivity results has been underlined.

Possible further developments of this beam interruption benchmark are being discussed and a proposal will be presented in the near future.

REFERENCES

[1] D'Angelo, A. (ENEA) and F. Gabrielli (Polytechnic of Turin), *Benchmark on Beam Interruptions in an Accelerator-driven System – Final Report on Phase I Calculations*, OECD Nuclear Energy Agency, NEA/NSC/DOC(2003)17, ISBN 92-64-02138-8. See also A. D'Angelo (on behalf of all the benchmark participants) and F. Gabrielli, "Benchmark on Beam Interruptions in a Lead-bismuth-cooled and MOX-fuelled Accelerator-driven System", *Proc. of GLOBAL 2003*, and "Atoms for Prosperity: Updating Eisenhower's Global Vision for Nuclear Energy", *American Nuclear Society and European Nuclear Society (ANS/ENS) International Winter Meeting Embedded Topical Meeting*, New Orleans, Louisiana, 16-20 November pp. 661-666 (2003).

[2] Baron, D., "About the Modelling of Fuel Thermal Conductivity Degradation at High Burn-up Accounting for Recovering Process with Temperature", *Proc. of the Seminar on Thermal Performance of High Burn-up LWR Fuel*, Cadarache, France, 3-6 March 1998.

[3] Baron, D., "Fuel Thermal Conductivity: A Review of the Modelling Available for UO_2, $(U\text{-}Gd)O_2$ and MOX Fuel", *Proc. of the Seminar on Thermal Performance of High Burn-up LWR fuel*, Cadarache, France, 3-6 March 1998.

[4] Ross, A.M. and R.L. Stoute, *Heat Transfer Coefficient Between UO_2 and Zircaloy-2*, AECL-1552 (1962).

[5] The RELAP5 Code Development Team, *RELAP5/MOD3 Code Manual. Volume I: Code Structure, System Models and Solution Methods*, NUREG/CR-5535 (1995).

[6] Fink, J.K., "Thermophysical Properties of Uranium Dioxide", *Journal of Nuclear Materials*, 279, 1-18, Elsevier (2000).

[7] Carbajo, J.J., G.L. Yoder, S.G. Popov, V.K. Ivanov, "A Review of Thermophysical Properties of MOX and UO_2 Fuels", *Journal of Nuclear Materials*, 299, 181-198, Elsevier (2001).

TABLES

Table 1. Fuel temperature variations in PDS-XADS cases

Beam interruption (s)	Maximum fuel temperature variations (K)		
	Average pin		Hottest pin
	No decay heat condition (Phase I of benchmark)	6% of decay heat	6% of decay heat
1	**~ 67 ± 2**	**~ 63 ± 2**	**~ 89 ± 4**
6	~ 286 ± 9	~ 270 ± 8	~ 390 ± 18

Table 2. Coolant temperature variations in PDS-XADS cases

Beam interruption (s)	Maximum outlet coolant temperature variations (K)		
	Average pin		Hottest pin
	No decay heat condition (Phase I of benchmark)	6% of decay heat	6% of decay heat
1	~ 13	~ 12	~ 20
6	**~ 62**	**~ 58**	**~ 80**

Table 3. Fuel temperature variations in MYRRHA cases

Beam interruption (s)	Maximum fuel temperature variations (K)		
	Average pin		Hottest pin
	No decay heat condition (Phase I of benchmark)	6% of decay heat	6% of decay heat
1	**–**	**~ 190 ± 13**	**~ 260 ± 21**
6	–	~ 825 ± 58	~ 1220 ± 98

Table 4. Coolant temperature variations in MYRRHA cases

Beam interruption (s)	Maximum outlet coolant temperature variations (K)		
	Average pin		Hottest pin
	No decay heat condition (Phase I of benchmark)	6% of decay heat	6% of decay heat
1	–	~ 31	~ 50
6	**–**	**~ 92**	**~ 140**

FIGURES

Figure 1. Initial (steady-state) XADS average pin axial temperature distributions

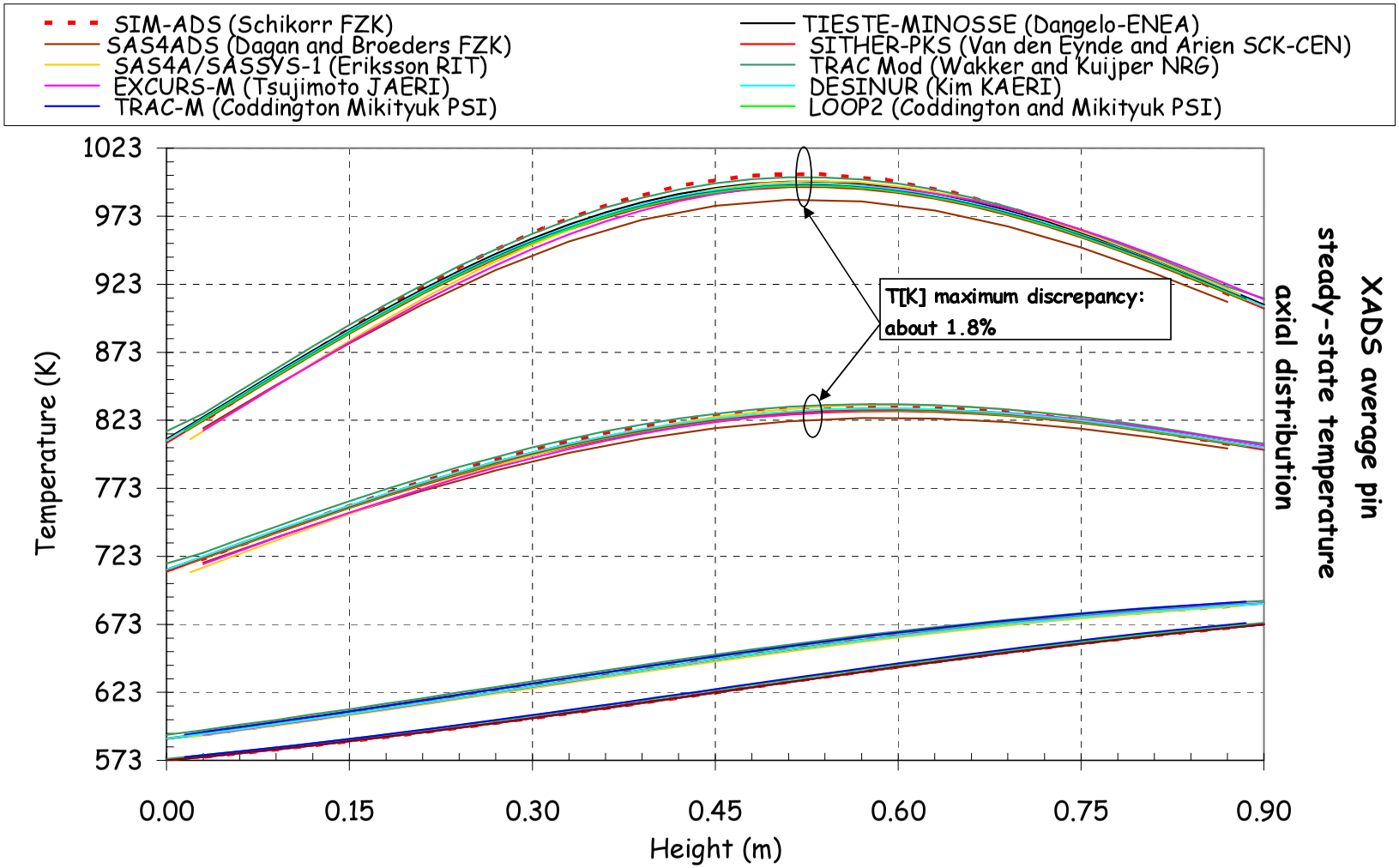

Figure 2. Initial (steady-state) XADS hottest pin axial temperature distributions

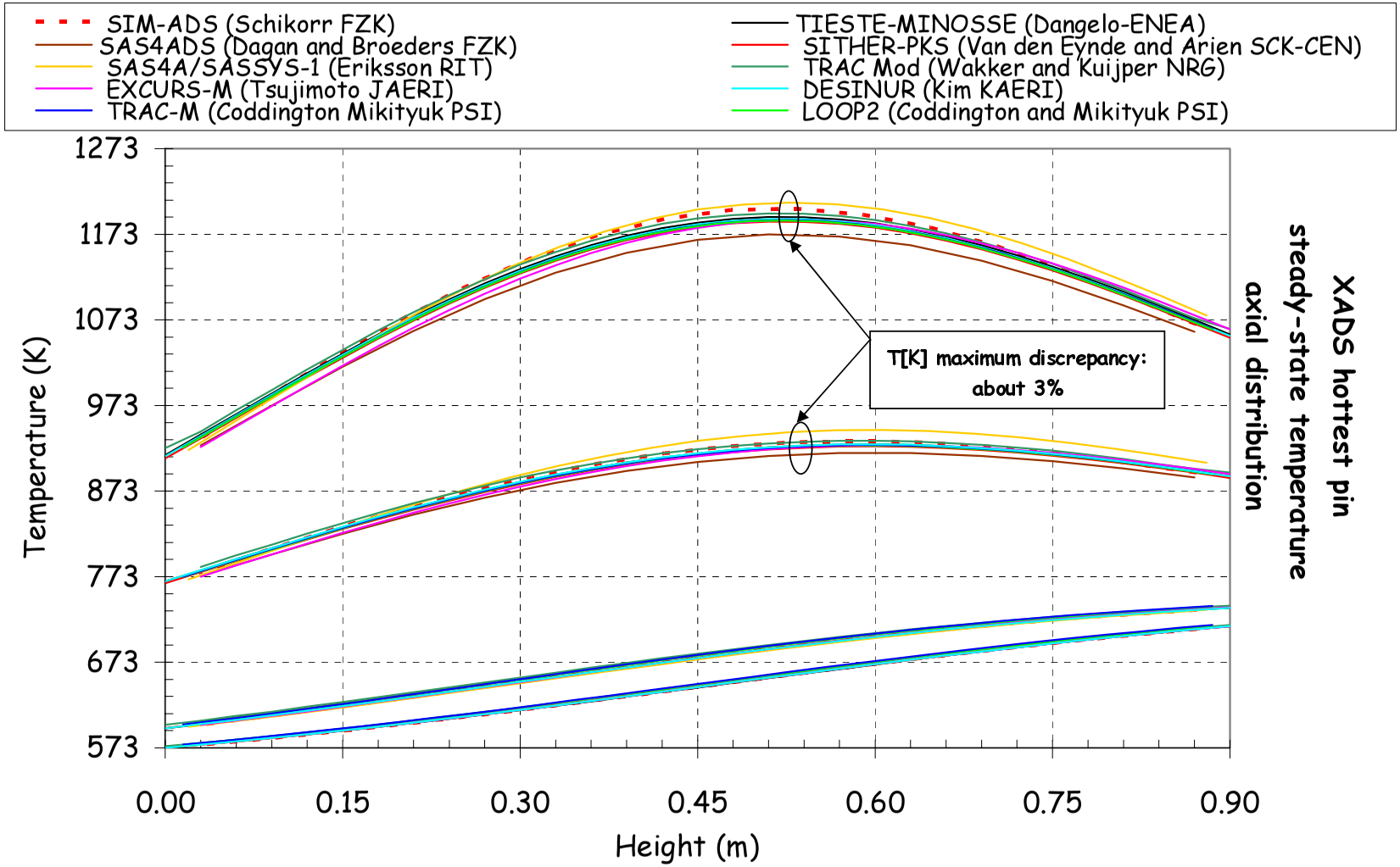

Figure 3. Initial (steady-state) MYRRHA average pin axial temperature distributions

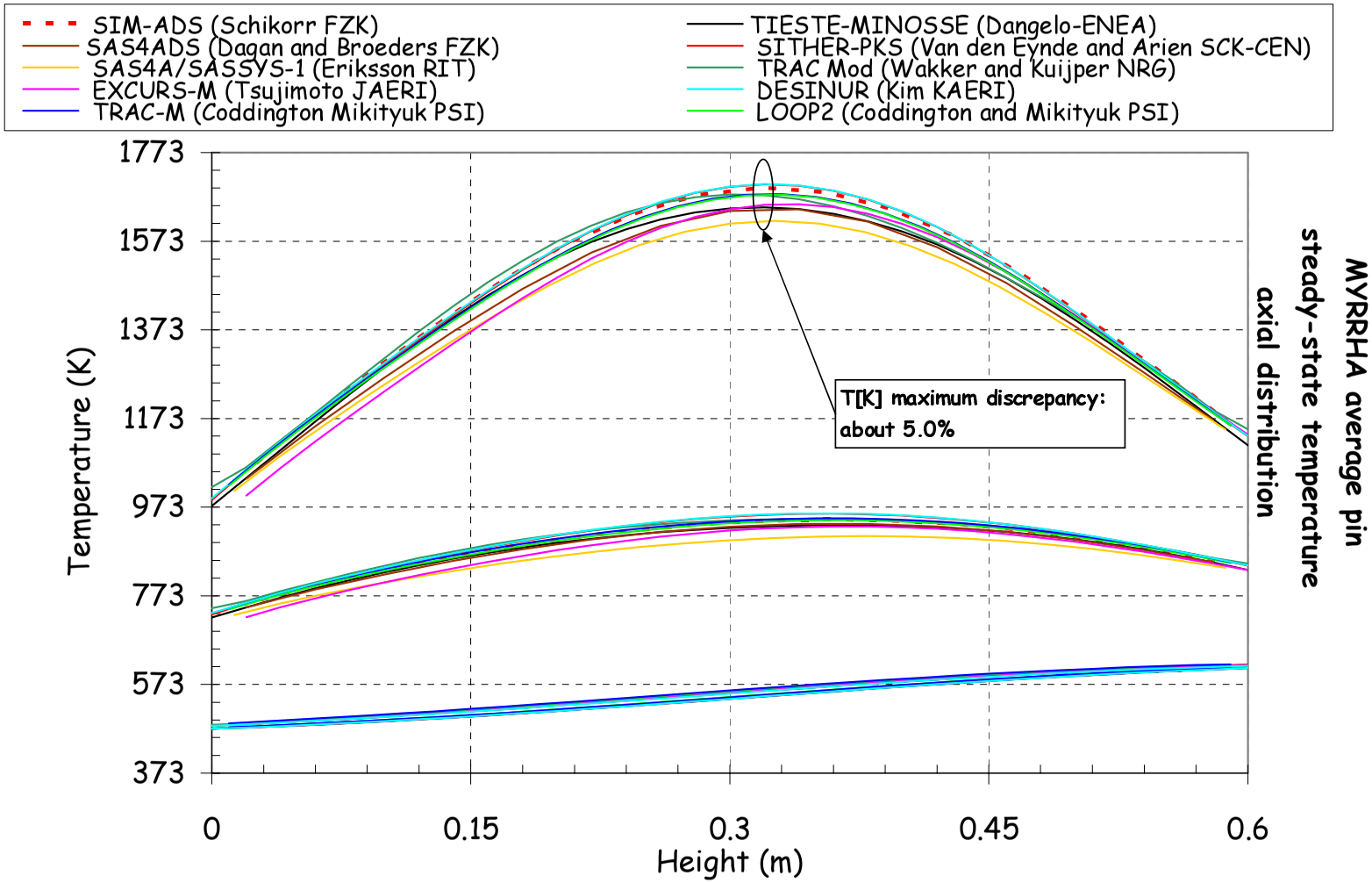

Figure 4. Initial (steady-state) MYRRHA hottest pin axial temperature distributions

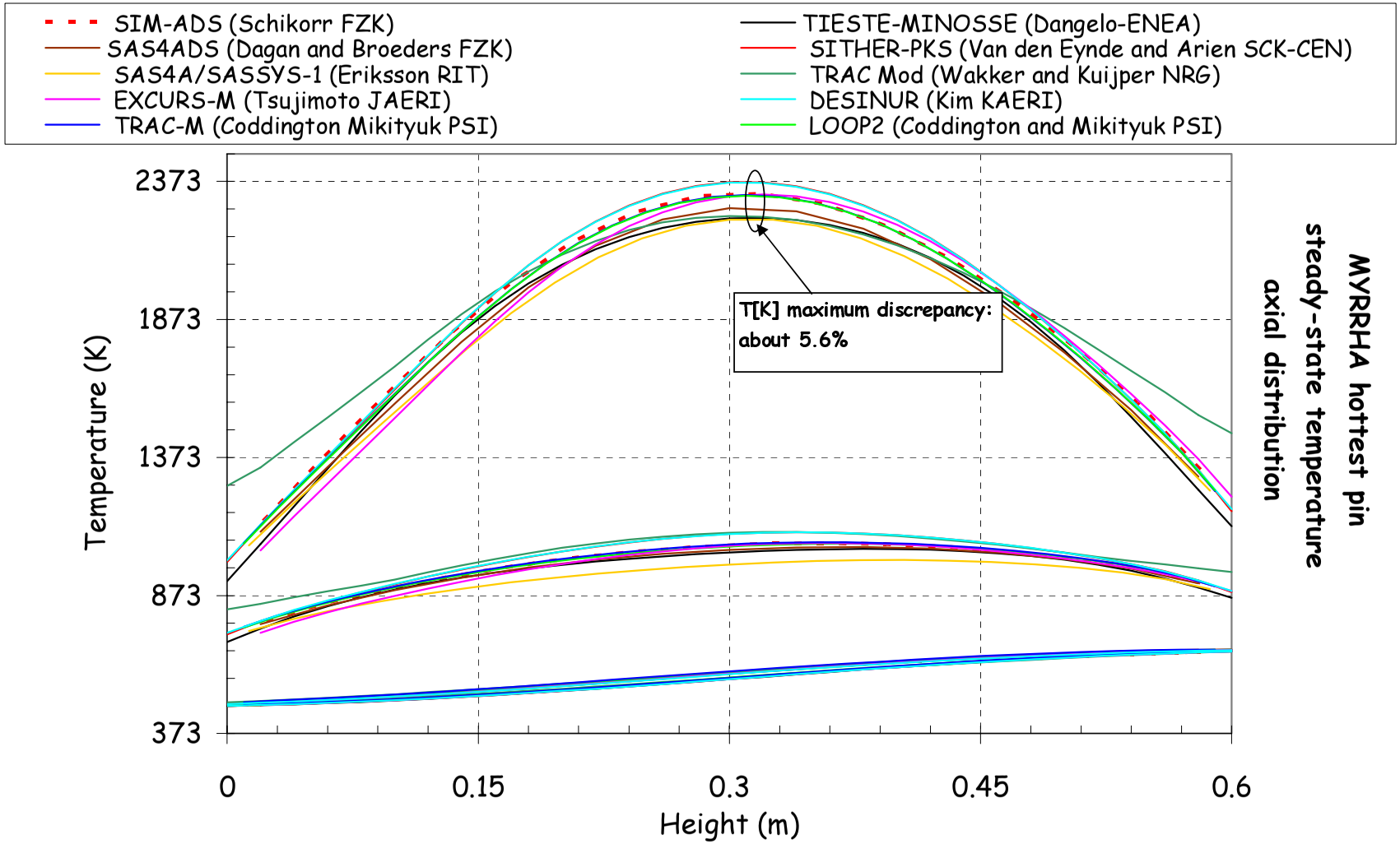

Figure 5. XADS average pin fuel centreline temperature transients induced by beam interruptions of different duration: 1 s and 6 s

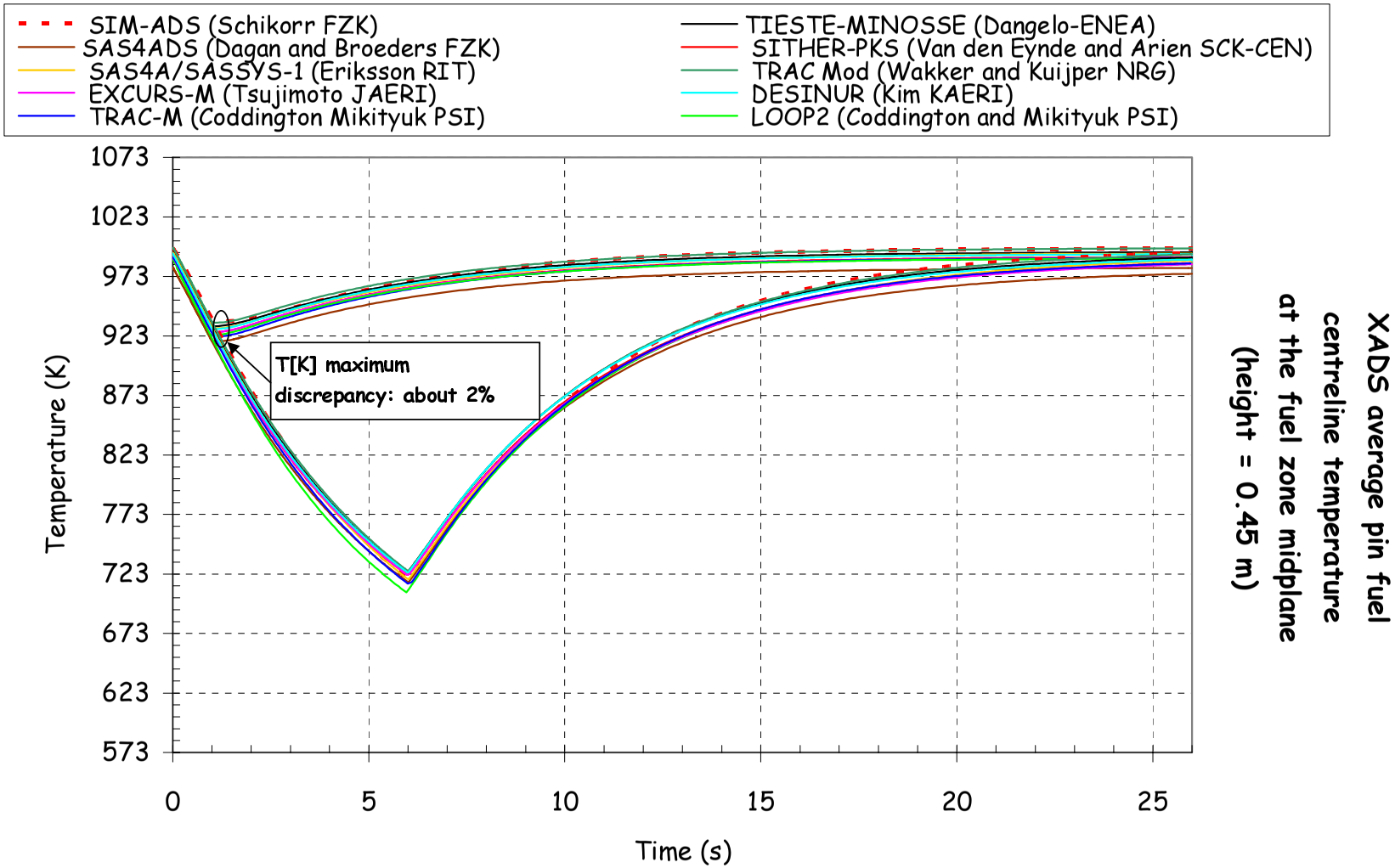

Figure 6. XADS hottest pin fuel centreline temperature transients induced by beam interruptions of different duration: 1 s and 6 s

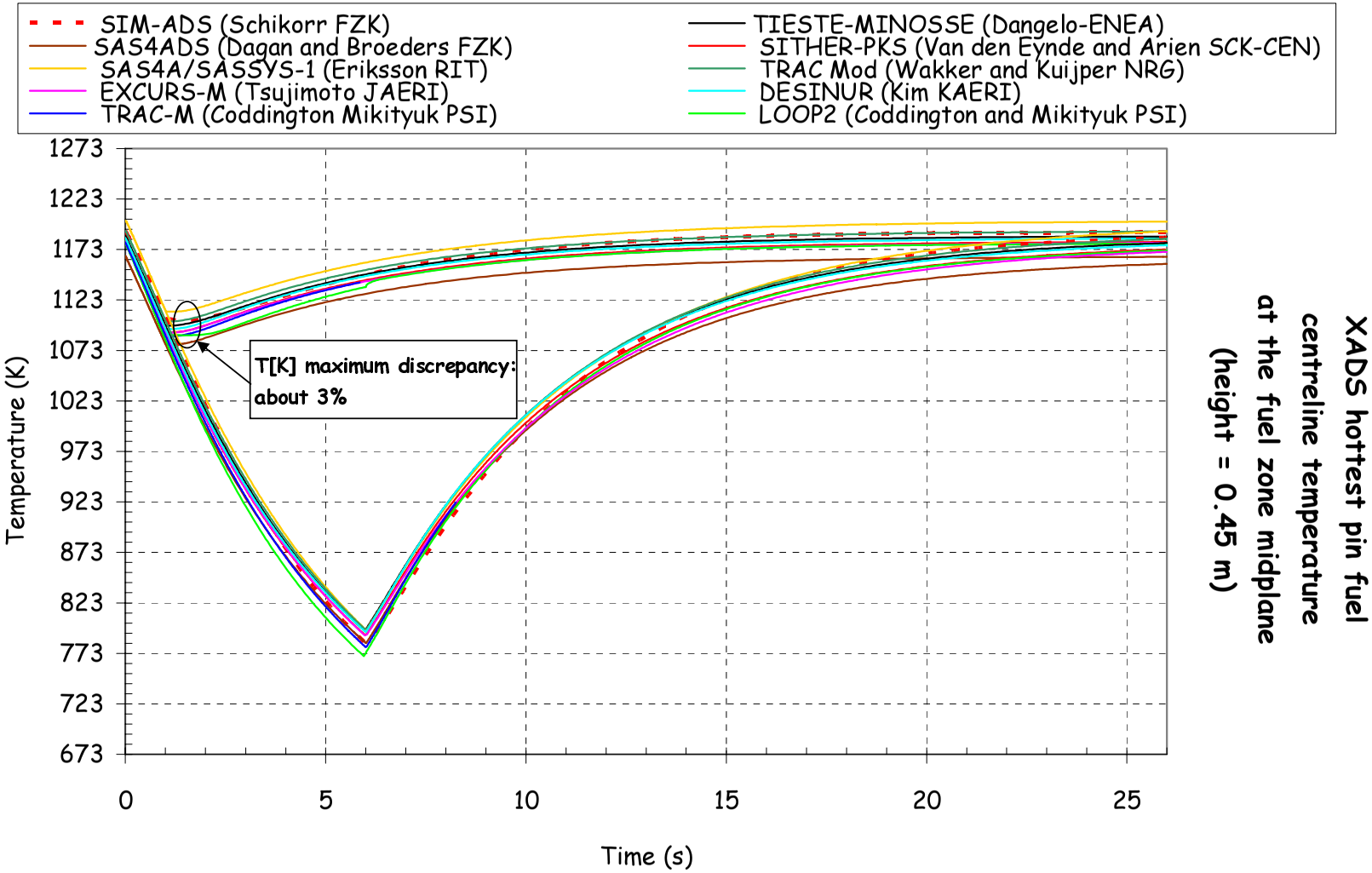

XADS hottest pin fuel centreline temperature at the fuel zone midplane (height = 0.45 m)

Figure 7. MYRRHA average pin fuel centreline temperature transients induced by beam interruptions of different duration: 1 s and 6 s

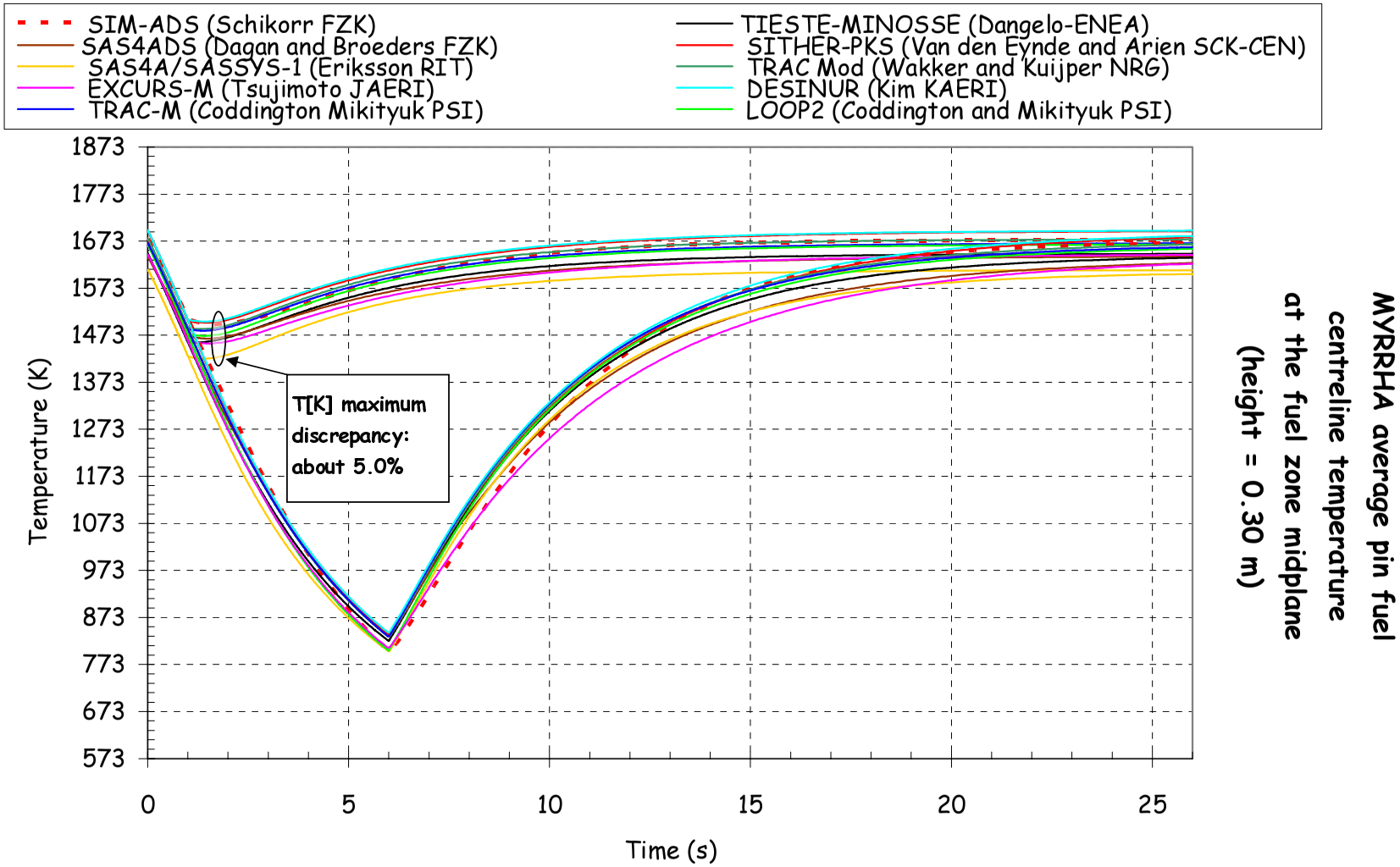

Figure 8. MYRRHA hottest pin fuel centreline temperature transients induced by beam interruptions of different duration: 1 s and 6 s

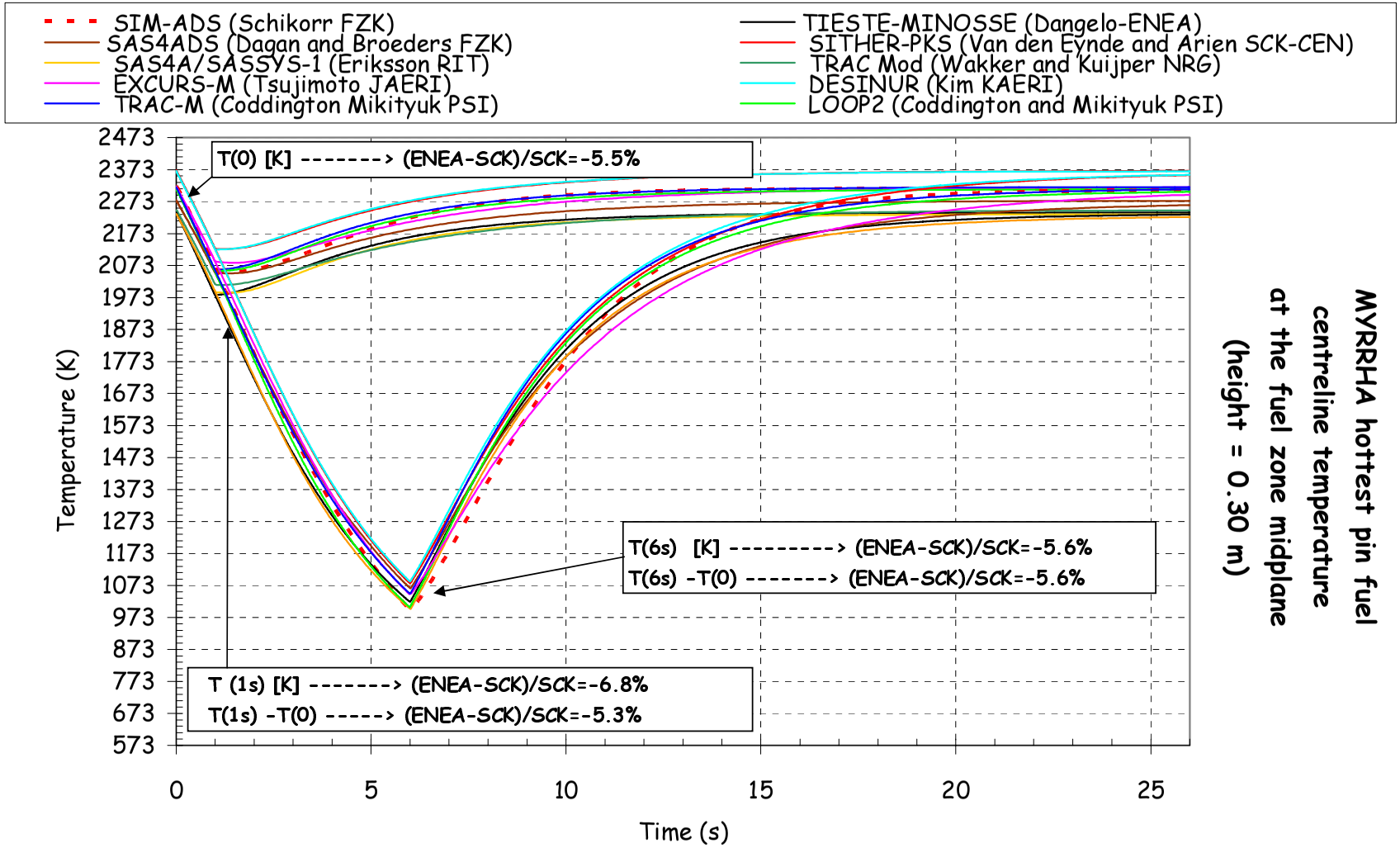

Figure 9. XADS average pin outlet coolant temperature transients induced by beam interruptions of different duration: 1 s and 6 s

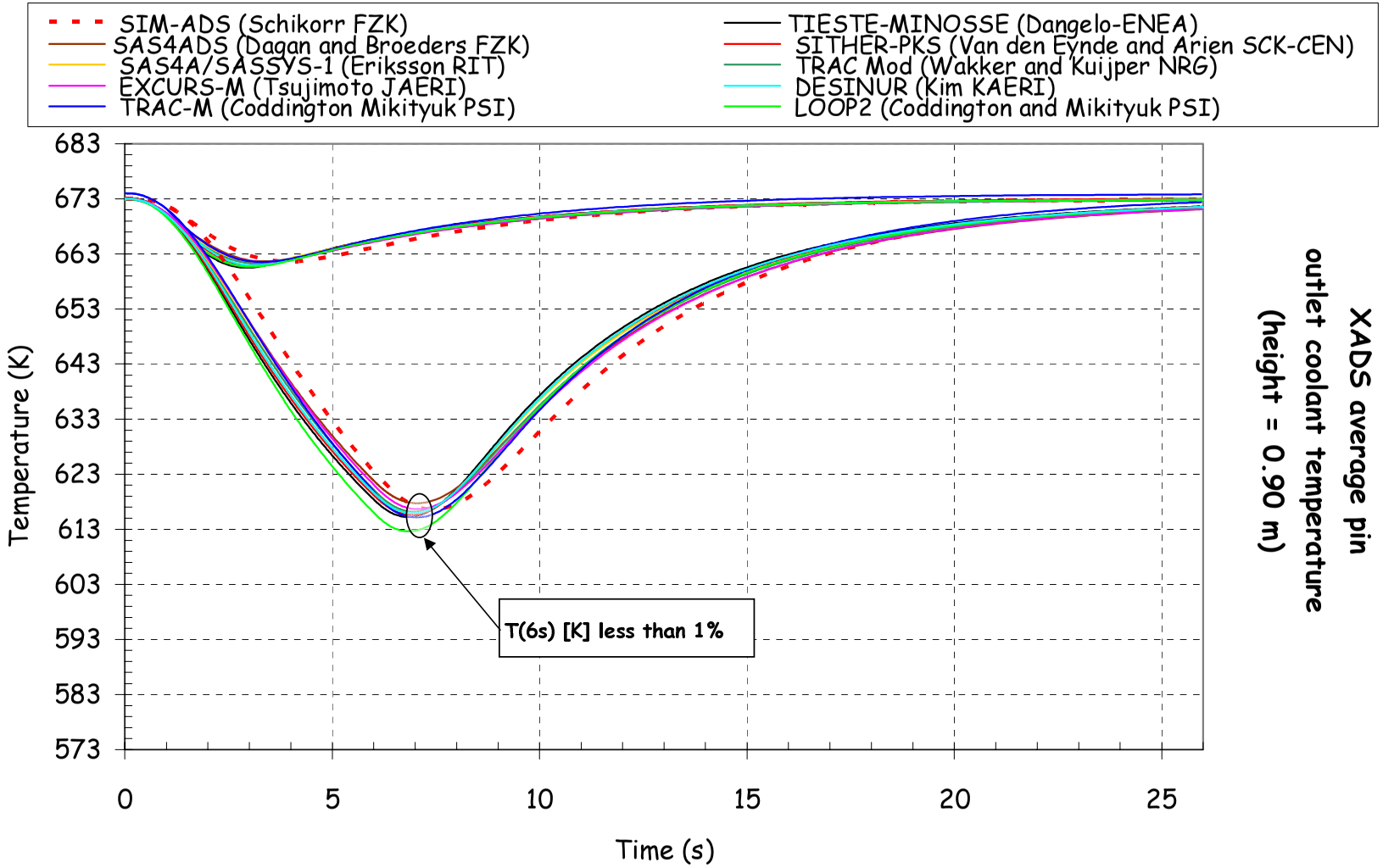

Figure 10. XADS hottest pin outlet coolant temperature transients induced by beam interruptions of different duration: 1 s and 6 s

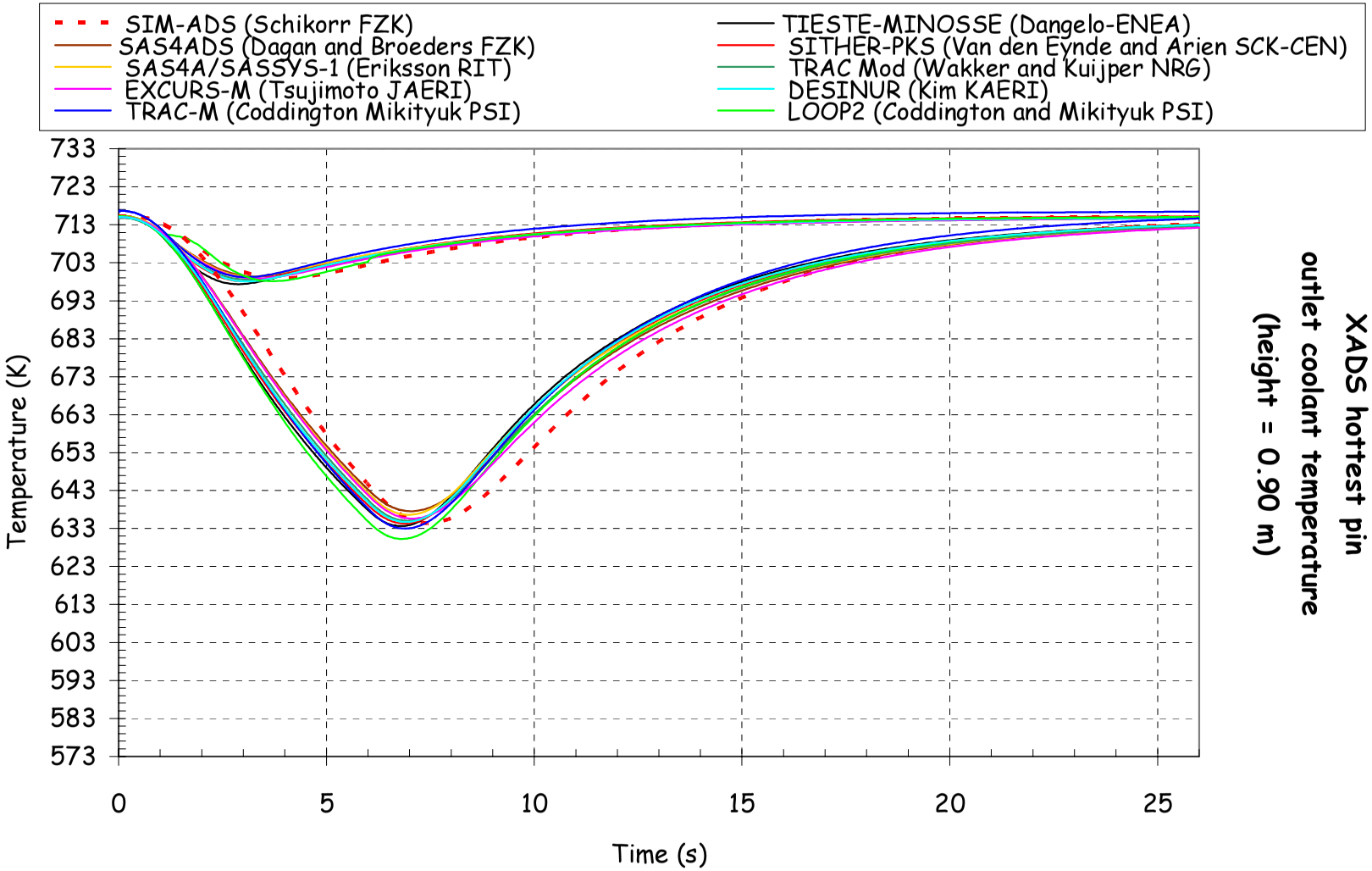

Figure 11. MYRRHA average pin outlet coolant temperature transients induced by beam interruptions of different duration: 1 s and 6 s

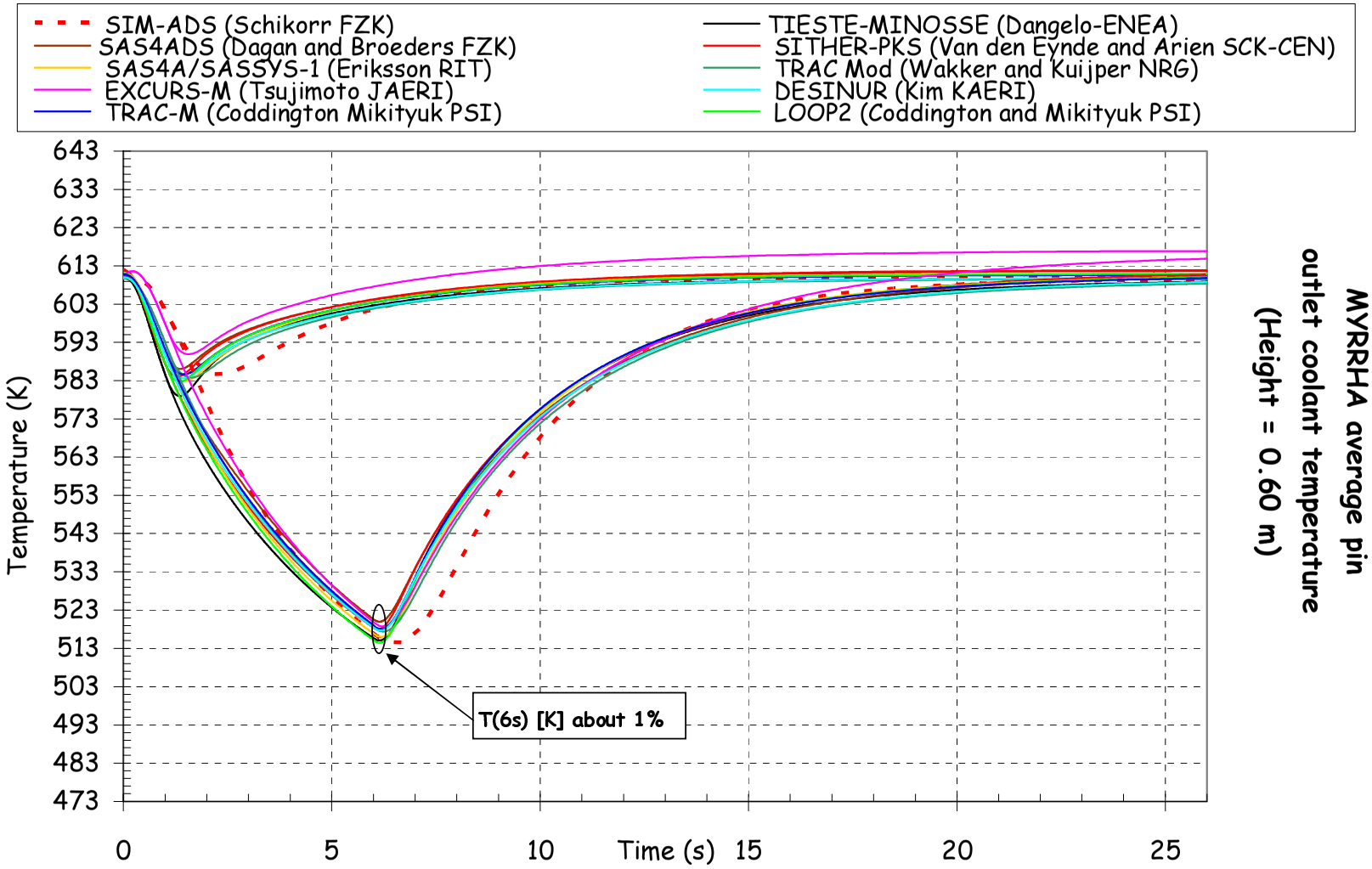

Figure 12. MYRRHA hottest pin outlet coolant temperature transients induced by beam interruptions of different duration: 1 s and 6 s

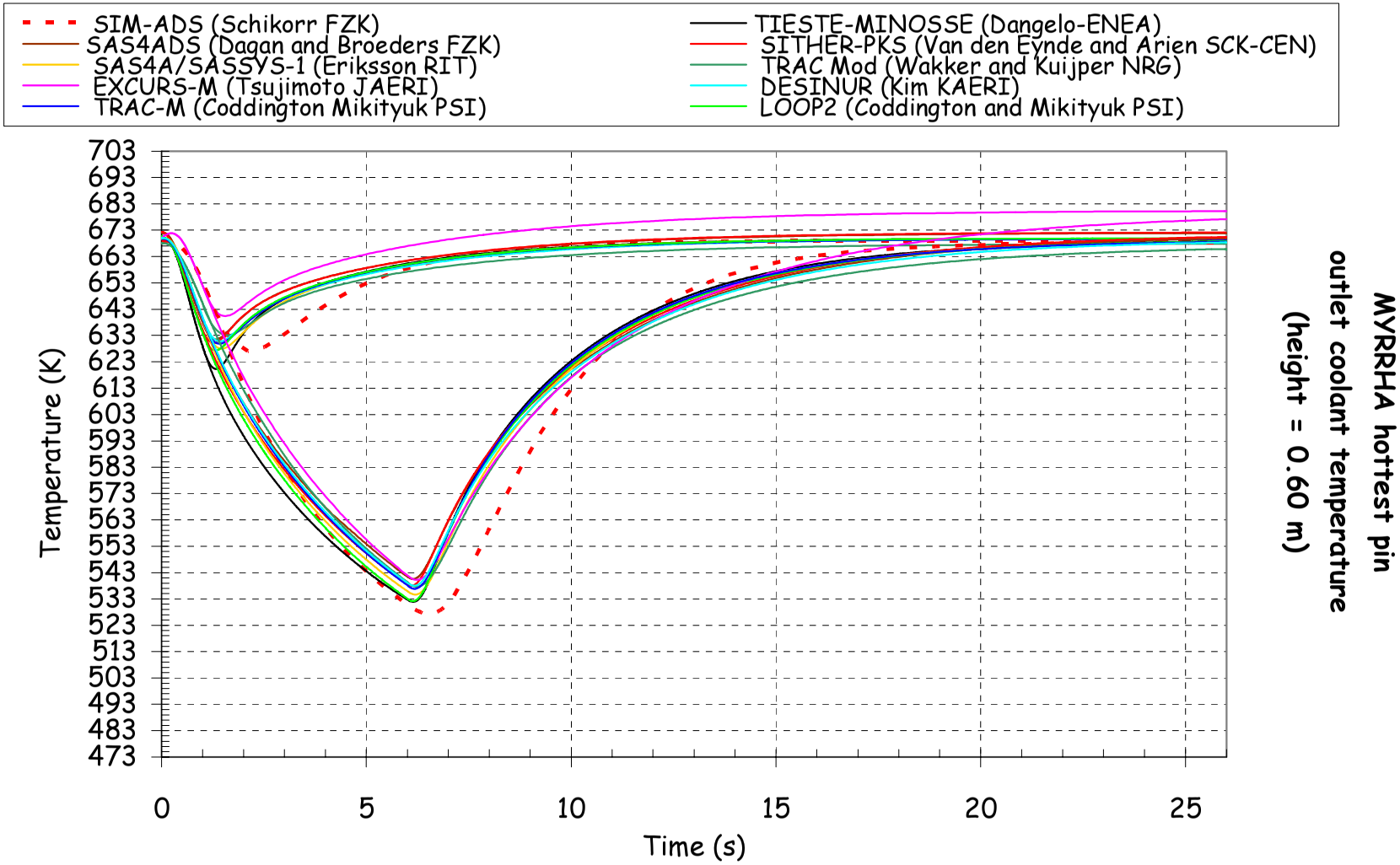

Figure 13. Impact of different assumptions on the XADS average pin fuel centreline temperature axial distribution

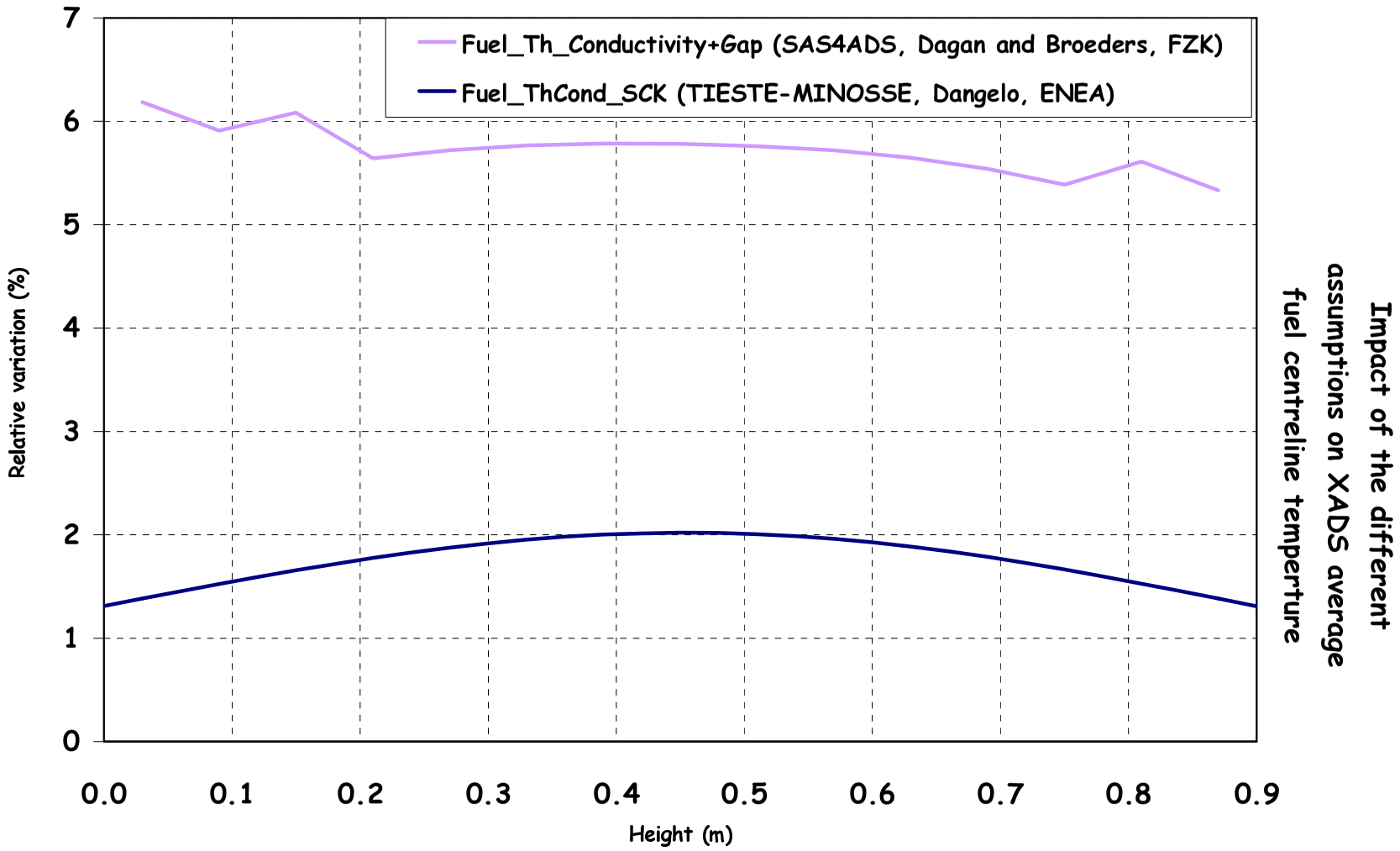

Figure 14. Impact of different assumptions on the XADS average pin fuel centreline temperature transient induced by 1 s of beam interruption

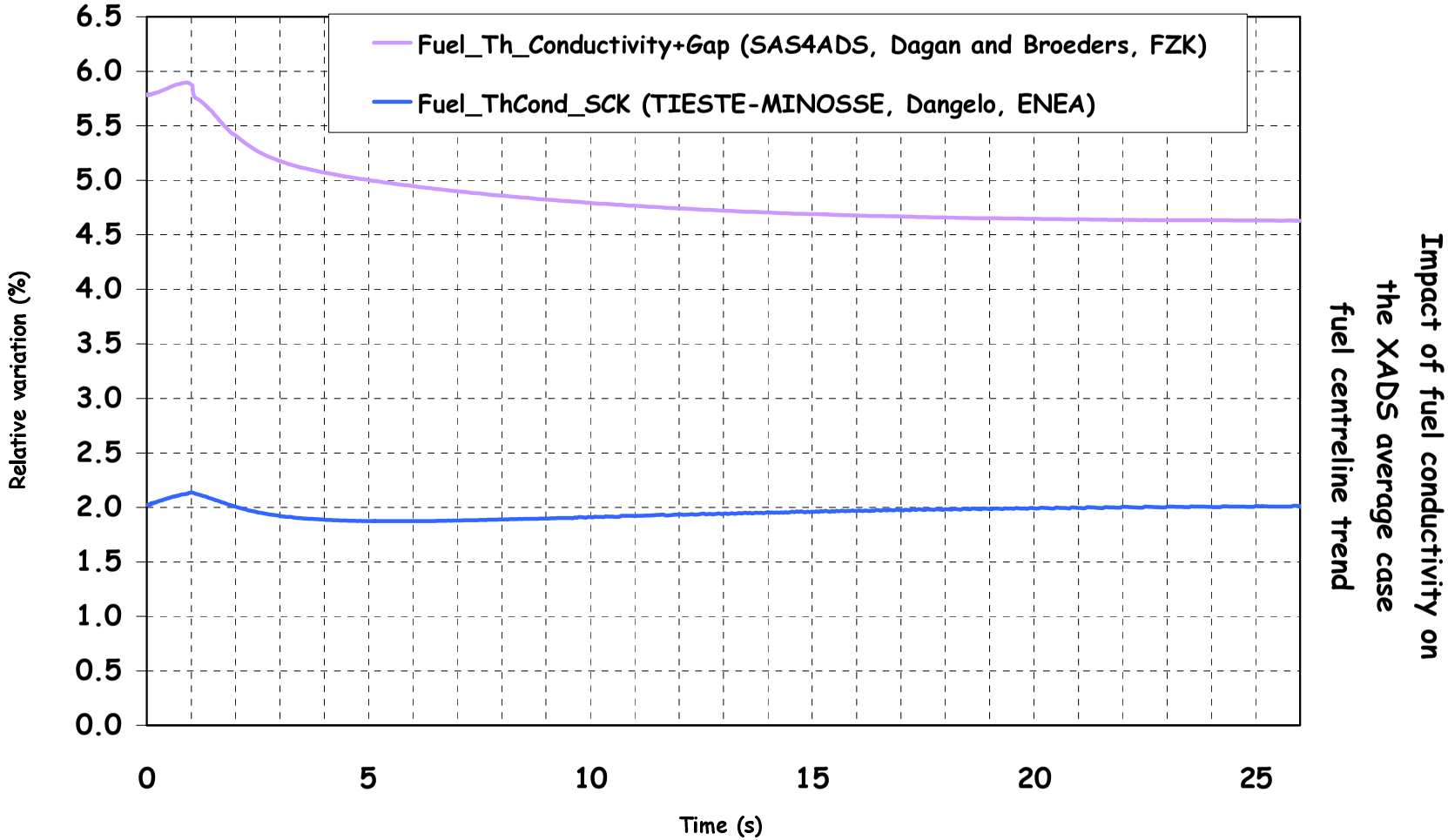

Impact of fuel conductivity on the XADS average case fuel centreline trend

Figure 15. Some evaluations and models for the 100% theoretical density (TD) MOX fuel thermal conductivity

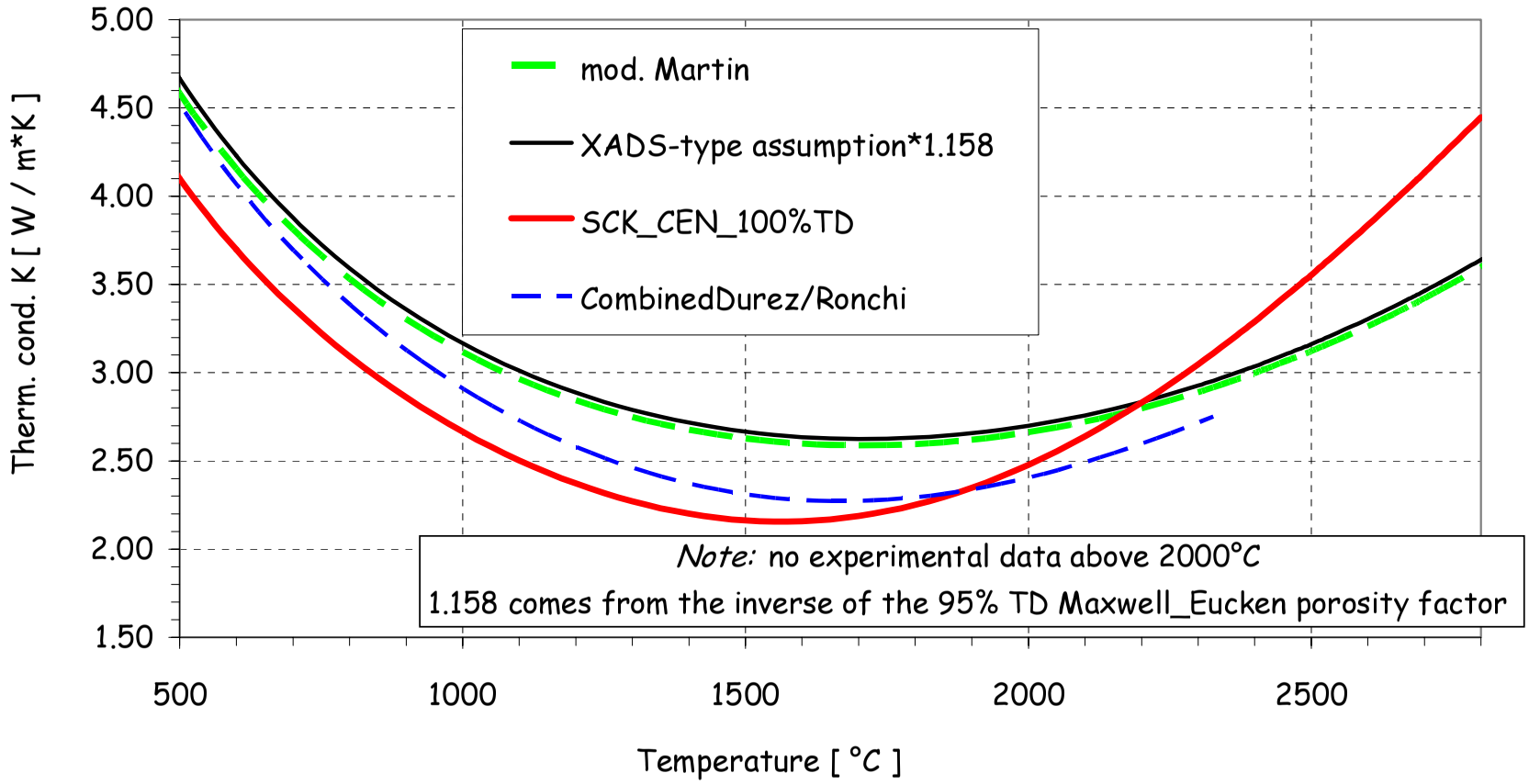

Figure 16. Impact of different assumptions on the XADS hottest pin fuel centreline temperature axial distribution

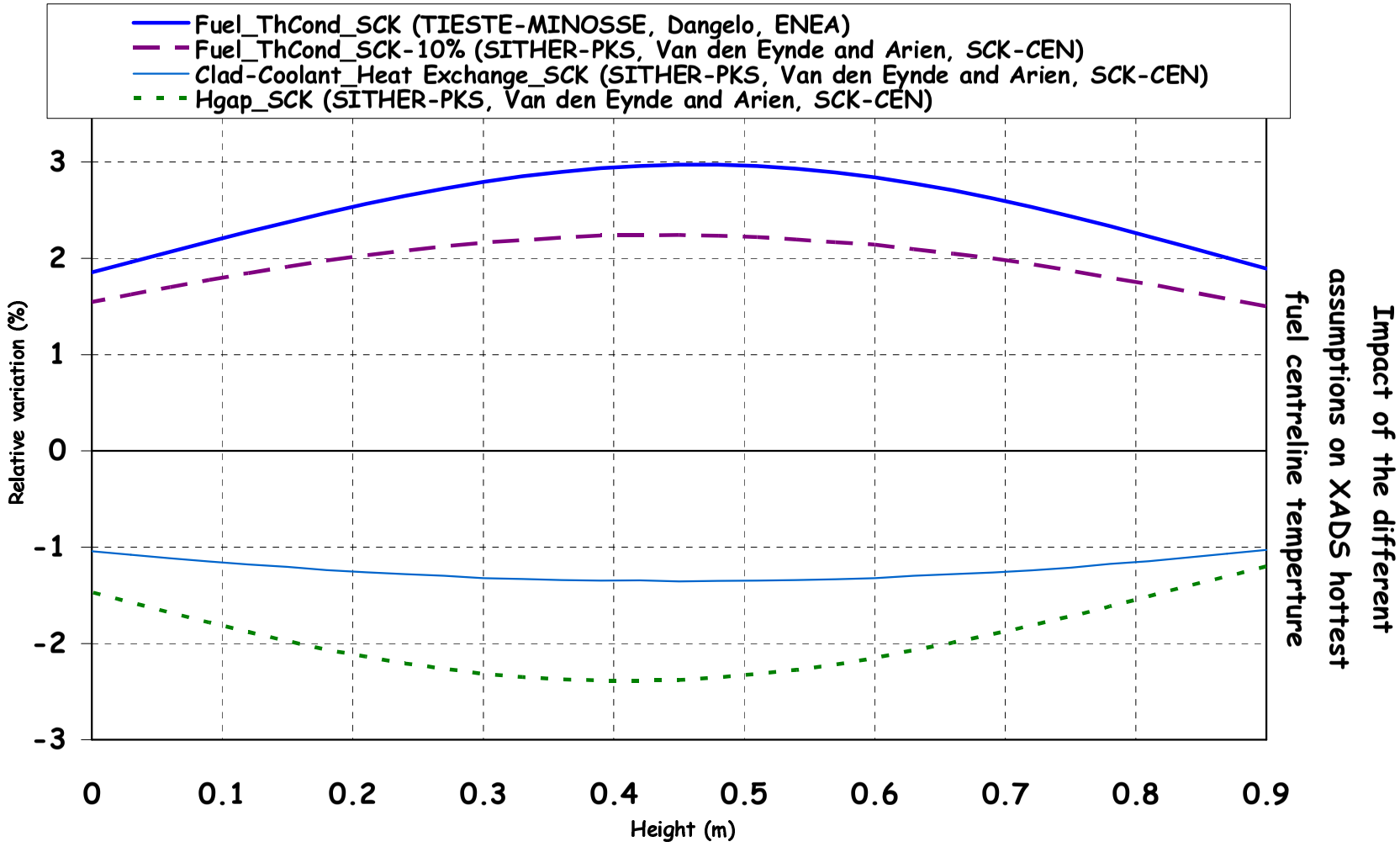

Figure 17. Impact of different assumptions on the XADS hottest pin fuel centreline temperature transient induced by 1 s of beam interruption

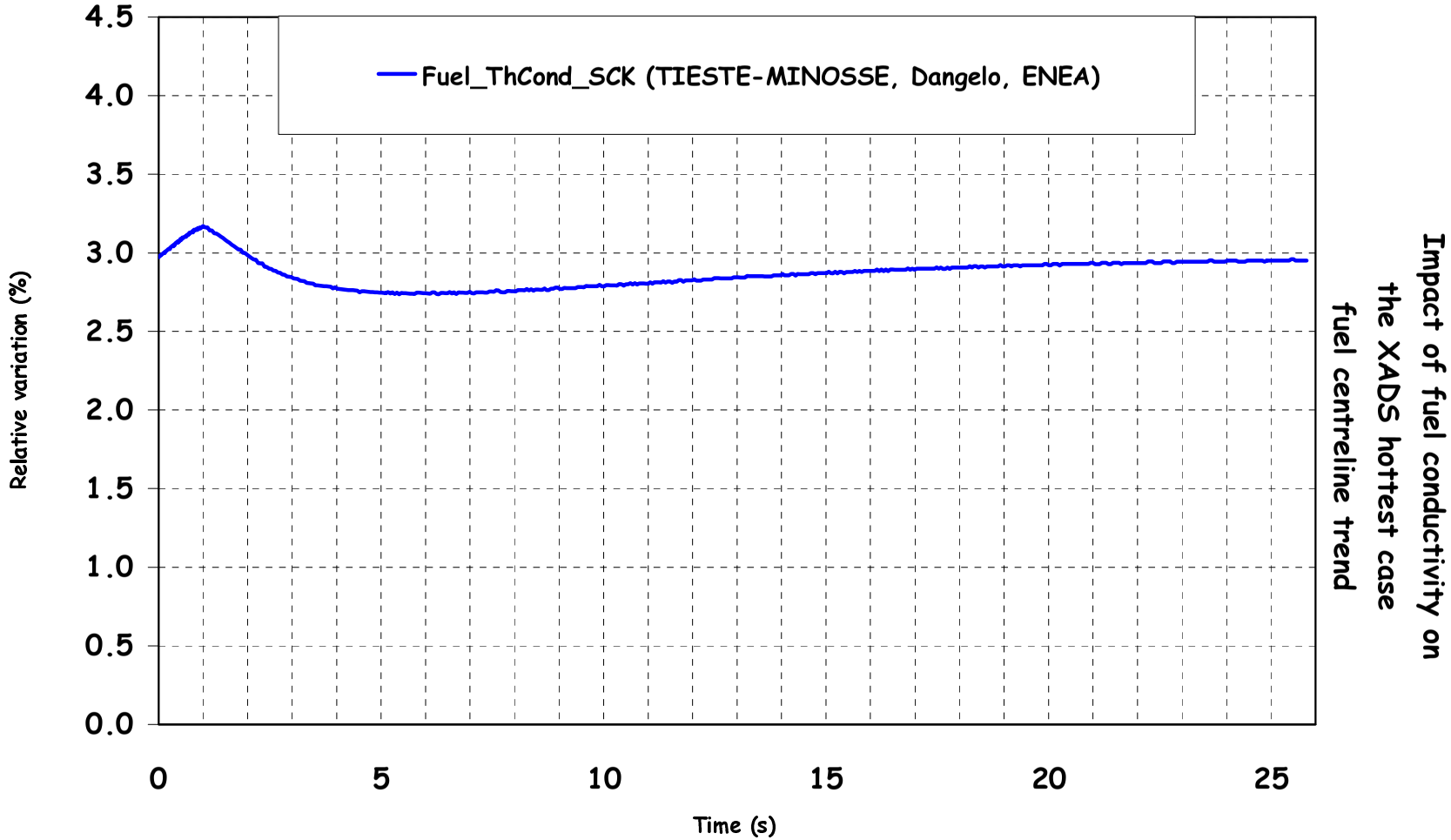

Impact of fuel conductivity on the XADS hottest case fuel centreline trend

Figure 18. Impact of different assumptions on the MYRRHA average pin fuel centreline temperature axial distribution

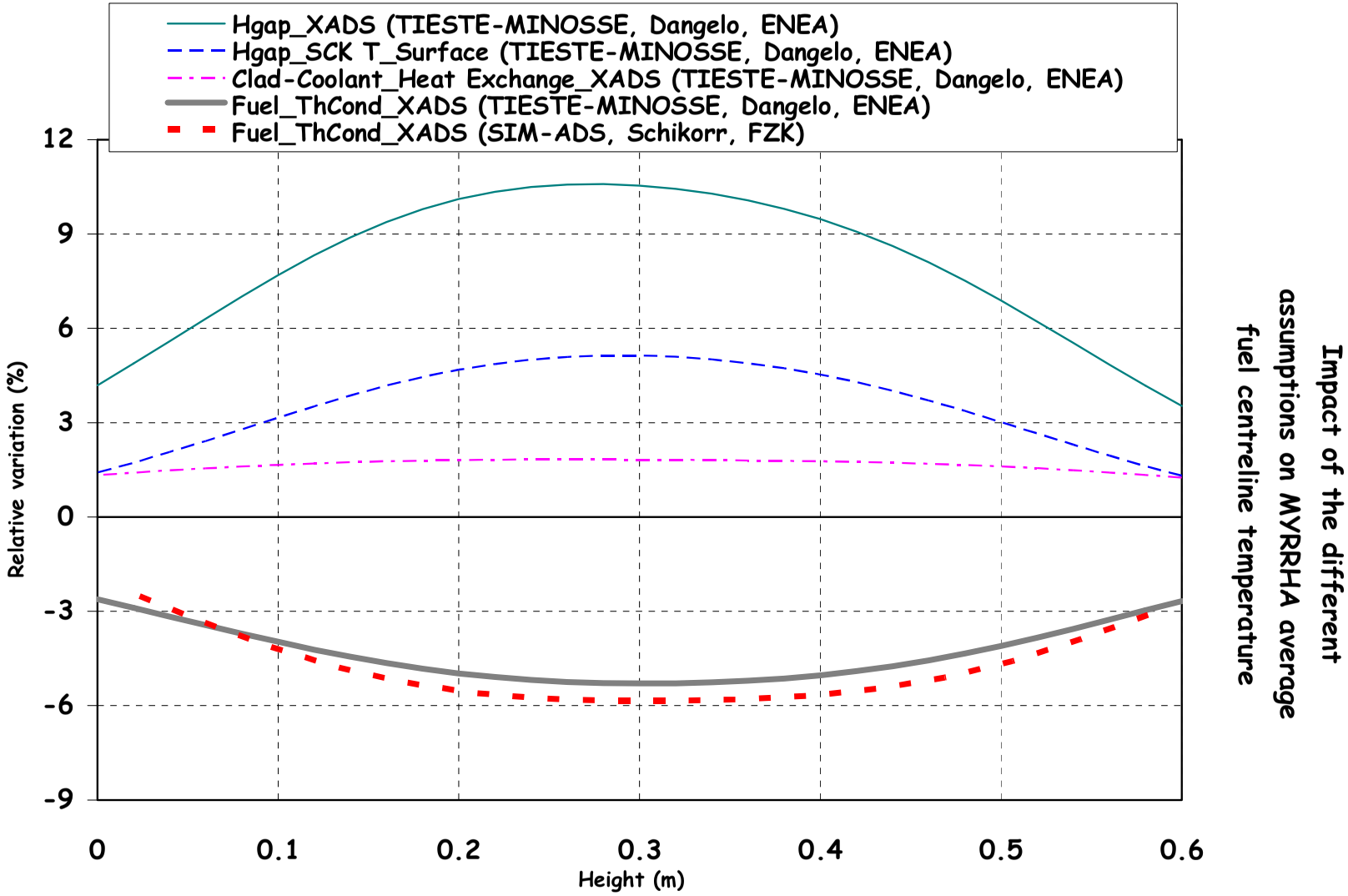

Figure 19. Impact of different assumptions on the MYRRHA average pin fuel centreline temperature transient induced by 1 s of beam interruption

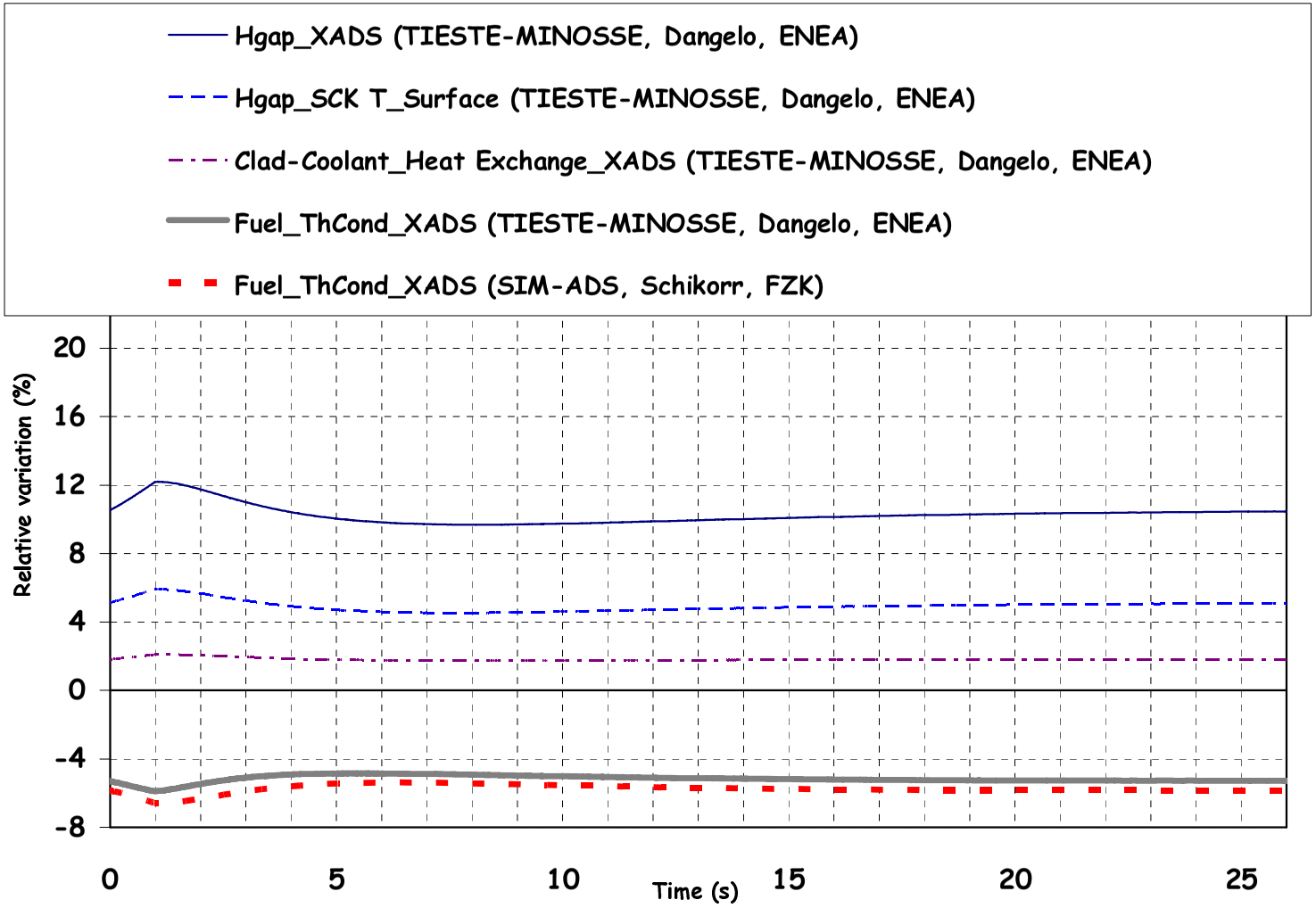

Impact of different assumptions on the MYRRHA average case fuel centreline trend

Figure 20. Impact of different assumptions on the MYRRHA hottest pin fuel centreline temperature axial distribution

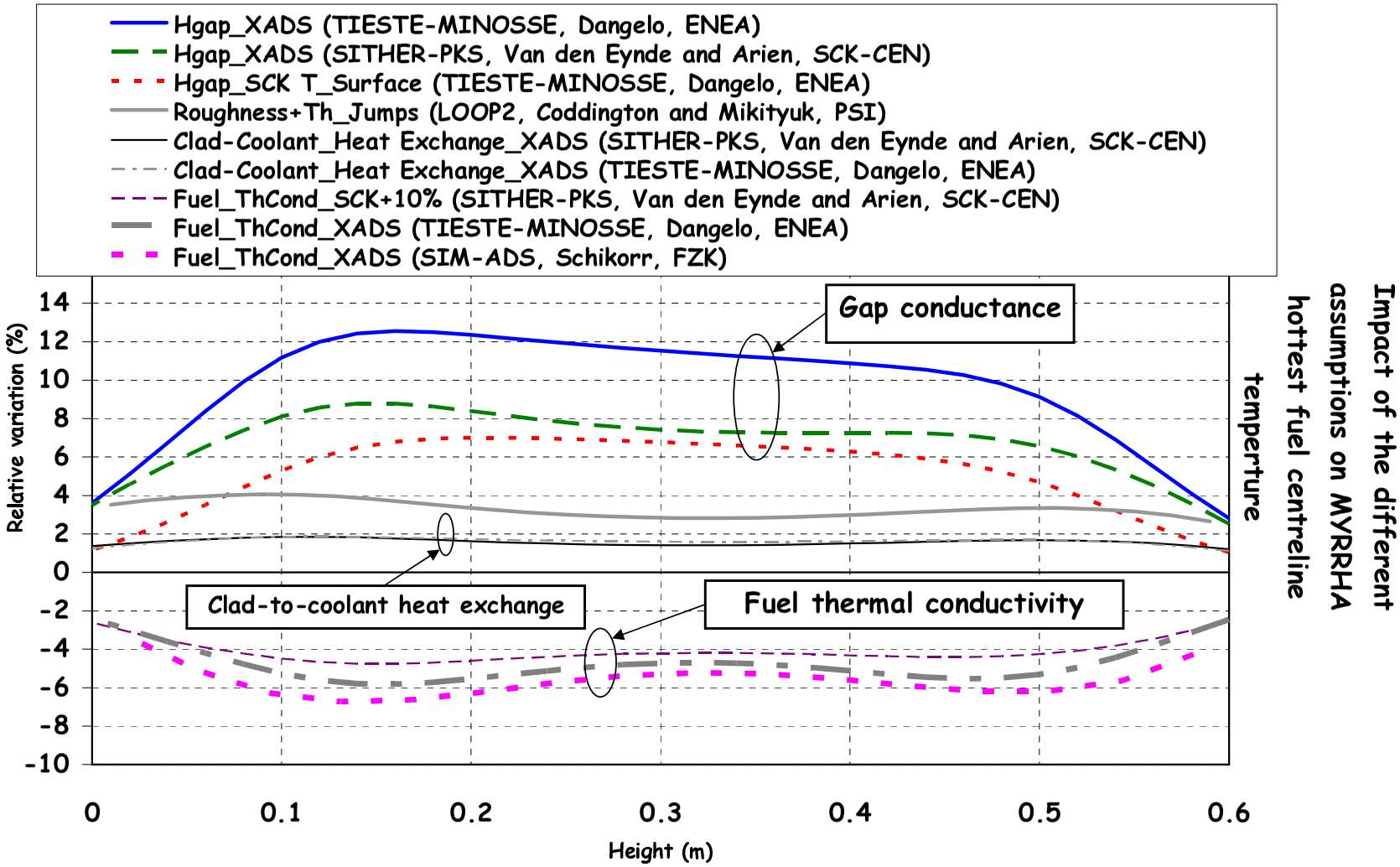

Impact of the different assumptions on MYRRHA hottest fuel centreline temperture

Figure 21. Impact of different assumptions on the MYRRHA hottest pin fuel centreline temperature transient induced by 1 s of beam interruption

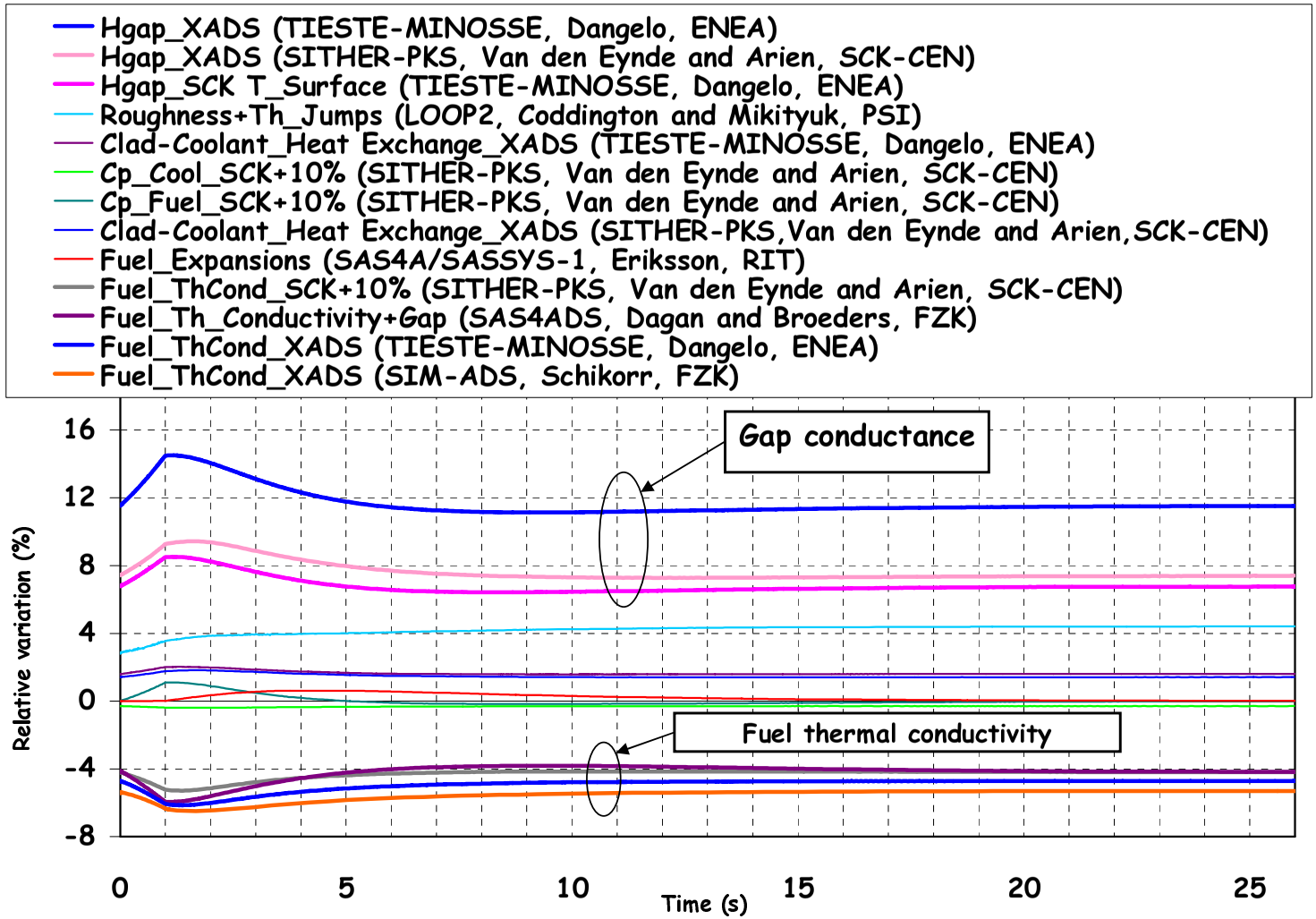

Impact of different assumptions on the MYRRHA hottest case fuel centreline trend

Figure 22. Impact of the MOX fuel specific heat on the MYRRHA hottest pin fuel centreline temperature variation induced by 1 s of beam interruption

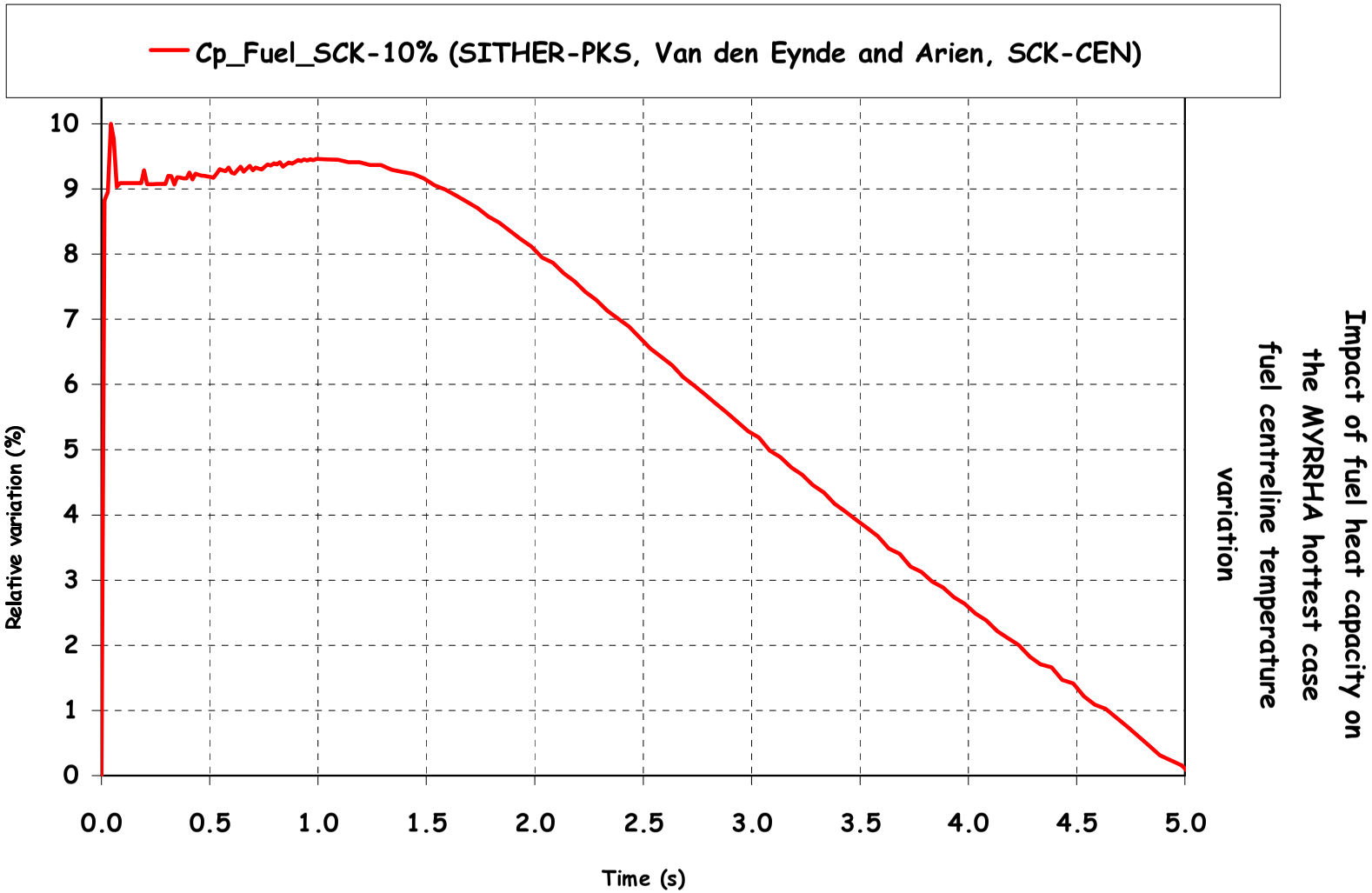

Impact of fuel heat capacity on the MYRRHA hottest case fuel centreline temperature variation

Figure 23. Impact of the fuel axial expansion on the MYRRHA hottest pin fuel centreline temperature variation induced by beam interruptions

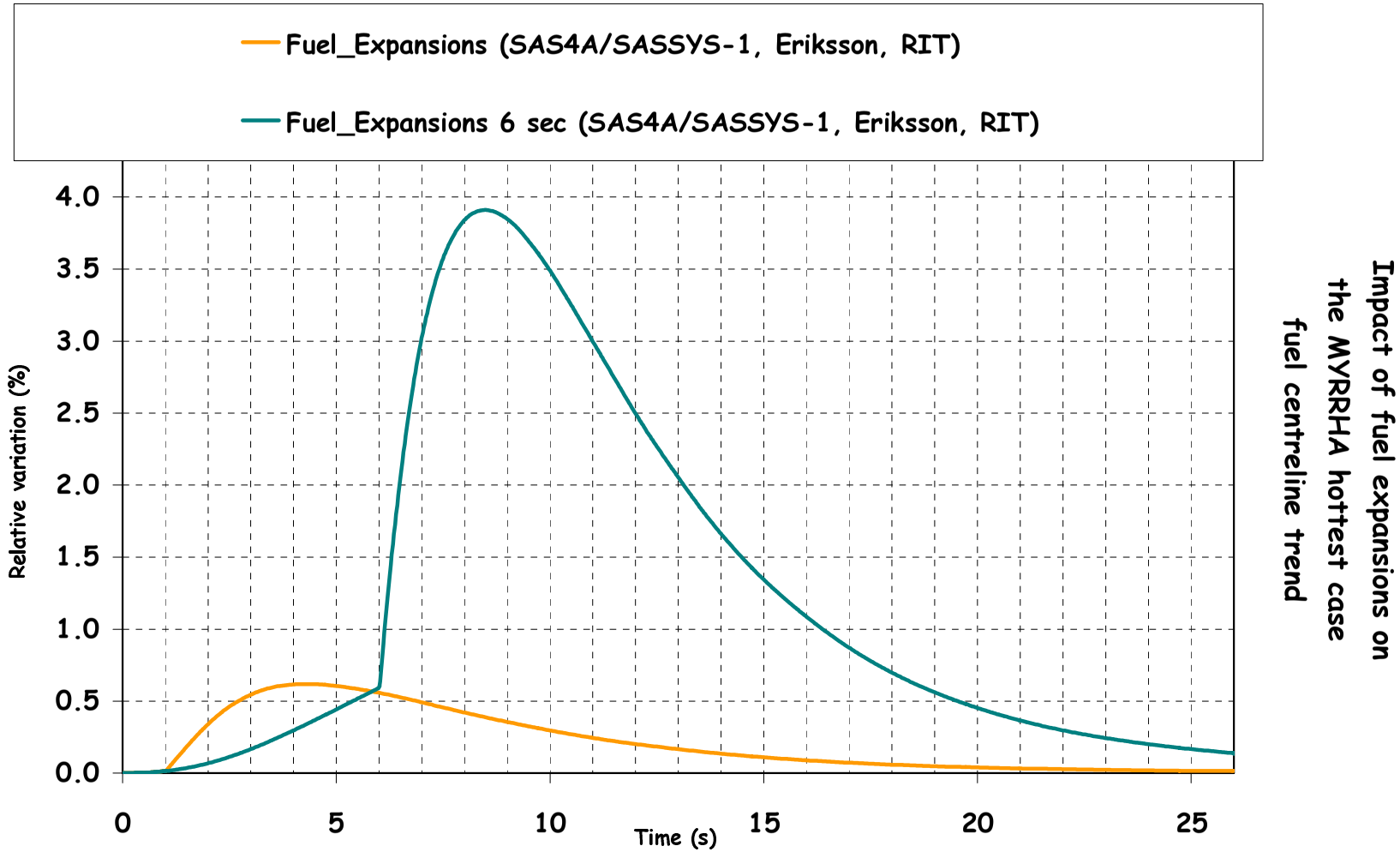

Appendix I

BEAM INTERRUPTIONS IN A LEAD-BISMUTH-COOLED AND MOX-FUELLED ACCELERATOR-DRIVEN SYSTEM

Benchmark Specification: Phase II

NEA/SEN/NSC/WPPT(2003)7
Working Party on Scientific Issues in Partitioning and Transmutation

A. D'Angelo, G. Bianchini and M. Carta
ENEA/Casaccia, P.O. Box 2400, 00100 Rome, Italy

B. Arien, V. Sobolev and G. Van den Eynde
SCK•CEN, Boeretang 200, Mol 2400, Belgium

F. Gabrielli
Politecnico di Torino, Dipartimento di Energetica, C.so Duca degli Abruzzi 24, 10129 Torino, Italy

Abstract

A second phase of benchmark calculations is proposed for the *Beam Interruptions in a Lead-bismuth-cooled and MOX-fuelled Accelerator-driven System* computational problem. This second phase of calculations aims to extend the beam interruption investigation to prototypical ADSs characterised by larger fuel power densities. To this aim, the computational benchmark is no longer limited to an XADS-type system, but has been extended to include a MYRRHA ADS-type.[1] Moreover, this second phase of calculations will investigate the impact on the fuel and coolant temperature results of different assumptions relevant to heat transfer correlations, material properties, fuel channel geometry or any other thermal-hydraulic calculation assumption. A further benchmark extension specifically devoted to irradiated fuel conditions is foreseen in the near future.

I. Introduction

The first phase of benchmark calculations relevant to transients induced by recovered beam interruptions in MOX-fuelled and lead-bismuth-cooled experimental ADS is complete. Phase I was a particularly clean comparative assessment of the different computation methods used to evaluate power and temperature transients induced by beam interruptions. In this context, the first phase of the benchmark can be considered successful, as the differences among all ten sets of results provided by the nine participants were physically negligible (< 3%).

The very good agreement among all the Phase I results is a stepping stone which has allowed to further develop the benchmark with the aim to investigate the impact of different and more complex calculation assumptions on fuel and coolant temperature trends. This report thus defines the goals and specifications of the second phase of benchmark calculations.

[1] MYRRHA is a small experimental ADS (i.e. SXADS) designed by SCK•CEN.

II. Description of the benchmark

Phase I of the beam interruption benchmark was a particularly clean and easy calculation exercise relevant to typical fresh fuel conditions only in an XADS. The second phase of calculations extends the calculations to very different fuel power density assumptions relevant not only to an XADS but also to a MYRRHA-type experimental ADS. In particular, this extension will allow to investigate the fuel and coolant temperature trends induced by beam interruptions in function of the following different power density assumptions:

- Case A – ~80 W/cm for an XADS-type average fuel pin.
- Case B – ~115 W/cm for an XADS-type hottest fuel pin.
- Case C – ~220 W/cm a MYRRHA-type average fuel pin.
- Case D – ~320 W/cm a MYRRHA-type hottest fuel pin.

In addition, a saturated decay heat level will be assumed at the beginning of the beam interruption. At the initial steady state and up to 0.001 s (the transient beginning) the decay heat production is assumed to be in equilibrium (i.e. the production rate of the decay heat precursors equals the decay rate) and the decay heat is assumed to be produced with the same axial shape as the fission power. The decay heat produced in the fuel at equilibrium will be assumed to be 6% of the total (fission plus decay) linear power with the axial distribution values reported in the annexed specifications. Due to the quite low impact of decay heat on the short-duration beam interruptions considered, participants are free to use their own model of residual heat precursor decay.

For each one of the four above-mentioned power density assumptions only two beam interruption durations will be considered, namely: 1 s and 6 s (instead of the four different beam interruption durations and the definitive trip investigated in Phase I). In fact, Phase I results have already indicated that the 1 s beam interruption is one of the most interesting durations for the investigation of fuel temperature variations (about 80 K in the case of the XADS average fresh fuel assumption). The 6 s beam interruption, on the other hand, is of greater interest with regard to investigating the impact of the calculation assumptions on the coolant temperature variations (about 60 K, 60% of the assumed initial coolant temperature between the outlet and inlet of the fuel channel).

The first set of calculation results (steady-state temperature distributions, temperature trends induced by 1 s and 6 s beam interruptions, respectively) for each one of the four power density cases (A, B, C and D) must be obtained assuming the simplified model specifications for an XADS-type (A and B) and a MYRRHA-type (C and D) experimental ADS that are reported in Annexes 1 and 2, respectively. The XADS-type specification for Case A differs from the Phase I specification [7] only for the 6% of decay heat assumption and for the reduced number of transients to be calculated (two instead of five). The XADS-type simplified specification for Case B (hottest fuel pin) differs from those of Case A only for:

- Fuel-pin total power (initial value): 10 246.0 W [8], instead of 7 203.6 W.
- Coolant outlet temperature (initial value): 715.0 K, instead of 673.0 K.

Practically, the coolant flow rate in Case B (hottest fuel pin) will have a result just slightly larger than that of Case A.

The linear power axial distribution to be assumed for Case B can be obtained by the values reported in Table 2 of Annex 1 by multiplying those values by 1.4223 (10 246 W/7 203.6 W).

III. Different calculation assumption investigations

In order to investigate the impact of different code and model calculation assumptions on fuel and coolant temperature trends, the benchmark participants are free to calculate a second set of results (steady-state temperature distributions, temperature trends induced by 1 s and 6 s beam interruptions for each one of the four power density cases) using all the correlations, channel geometry models or other thermal-hydraulic assumptions they think to be valid alternatives to or improvements upon those defined in the specifications found in Annexes I and II. In this case participants should also briefly (but completely) document their modifications to the benchmark thermal-hydraulic specification and analyse the origin of the significant fuel and coolant temperature variations.[2] In particular, so as to permit analysis of the origin of the temperature variation, participants who made more than one assumption different from the simplified model must group together variations concerning:

I) Fuel to clad heat transfer.

II) Fuel properties.

III) Clad to coolant heat transfer.

IV) Coolant properties.

V) Others.

The benchmark calculation should be repeated assuming no more than one set of different assumptions at one time. In this way, participants will detect the groups of assumptions that lead to significant variations in results. Similarly, if participants made more than one different assumption for assumption groups II) and IV) which have a significant impact on the temperature result they should repeat the calculations to separate the contributions of:

- Conductivity.
- Specific heat.
- Density.
- Others.

In this way, participants will detect the material property assumptions that lead to significant variations.

[2] Temperature variations larger than the 5% of the temperature values obtained by the benchmark specification and, in any case, larger than 5 degrees. Variations due only to time shifts in the result presentation, i.e. relevant to possible different origins of the temperature variation representation for possibly obtaining more detailed axial geometries, do not need to be considered significant.

IV. Beam interruptions and calculation result definition

It is assumed that the external neutron source that initially maintains the amplitude-factor of point kinetics as constant (steady-state conditions) drops suddenly to zero at one millisecond. Two benchmark problems are proposed for each of the four power density assumptions: beam interruptions of 1 s and 6 s. In order to model the two recovered beam interruptions, the external neutron source is assumed to be suddenly reset to the initial values of 1.001 s and 6.001 s, respectively.

The coolant temperature at the top of the fuel channel (height = 90 cm for XADS and 60 cm for MYRRHA) and the fuel centreline temperature at the fuel zone mid-plane (height = 45 cm for XADS and 30 cm for MYRRHA) are the main results requested of the benchmark participants. Results should be calculated at the initial conditions and for 26 s after the beam interruption time (from 0 s to 26.001 s).

Some additional results are also requested. These include:

- The fuel pin total power normalised to its initial value.
- The temperature distributions in the fuel channel at equilibrium initial conditions.
- Time-dependent temperatures in a few representative positions.

Specifically, it is requested that the following set (common to all the requested transients) of initial steady-state computed data be recorded:

- Axial distribution of the fuel centerline temperature.
- Axial distribution of the fuel surface temperature.
- Axial distribution of the clad surface temperature.
- Axial distribution of the coolant temperature.

It is further requested to record from time equal to 0 s to time equal to 26.001 s the following set of time-dependent calculation results relevant to each of the five proposed benchmarks:

- Fuel-pin total power normalised to its initial value.
- Fuel centreline temperature at the fuel zone mid-plane (height = 45 cm for XADS and 30 cm for MYRRHA ADS).
- Fuel surface temperature at the fuel zone mid-plane (height = 45 cm for XADS and 30 cm for MYRRHA ADS).
- Coolant temperature at the top of the fuel channel (height = 90 cm for XADS and 60 cm for MYRRHA).

Acknowledgements

The authors are particularly indebted to Paul Coddington and Hamid Abderrahim who contributed to the definition of the present. Many thanks also to Ron Dagan, Michael Schikorr and all those benchmark participants who proposed improvements to the Phase I benchmark specifications.

Annex I

XADS-TYPE SIMPLIFIED MODEL FOR FRESH FUEL AVERAGE CONDITIONS (CASE A)

A. D'Angelo, G. Bianchini, M. Carta and F. Gabrielli

Restriction: *The data in this annex are to be used by the benchmark participants only for this benchmark calculation and cannot be distributed to third parties. The data should not be used for design calculations. ENEA takes no liability whatsoever concerning the correctness of the data or the use thereof.*

I. Fuel channel geometry and power data

The 80 MWth[3] lead-bismuth-cooled XADS core is foreseen to charge 120 MOX fuel hexagonal assemblies, each one containing 90 active pins. The following simplified fuel element channel geometry[4] is assumed for the present benchmark in an XADS-type system.

Table 1. Fuel pin channel geometry

Fuel zone height	0.90 m
Inner fuel radius (inner hole radius)	0.9×10^{-3} m
Outer fuel radius	3.57×10^{-3} m
Inner clad radius	3.685×10^{-3} m
Outer clad radius	4.25×10^{-3} m
Coolant flow area	9.89×10^{-5} m^2
Coolant inlet temperature	573.0 K
Fuel pin total power (initial value for the "average" pin)	7 203.6W
Coolant outlet temperature (initial value)	673.0 K

The coolant movement in the XADS design is due to the lead-bismuth natural convection and the simultaneous action of the pumps. When pumps are working, the forced convection prevails on the lead-bismuth natural convection. Though the lead-bismuth flow rate variations due to the natural convection are essential to mitigate transients in which the coolant temperature tends to rise abnormally, it has a minor impact on the transients induced by beam trips [1]. Therefore, the corresponding mass flow rate variations during the beam interruption transients are neglected in the present benchmark proposal. Similarly, for the sake of simplicity, the inlet coolant temperature is also considered constant and equal to the initial value [2]. The channel model described above is given presuming that the coolant will be treated with a single lumped radial node and multiple axial nodes. In addition to the data provided in Table 1, the pin p value of 13.406×10^{-3} m is necessary to define the clad-coolant heat exchange by means of a Nusselt number correlation (see Section III).

[3] The thermal power produced in fuel elements is about 77.8 MW.

[4] Obtained taking into account only the fuel zone and forcing the geometry to solve an axial heterogeneity between MOX active fuel zone (87 cm) and UO_2 blanket zones (3 cm).

In Phase II of this benchmark a saturated decay heat level will be assumed at the beginning of the beam interruption. Practically, at the initial steady-state and up to 0.001 s (the transient beginning) the decay heat production is assumed to be in equilibrium (i.e. the production rate of the decay heat precursors equals the decay rate) and the decay heat is assumed to be produced with the same axial shape as the fission power. The decay heat produced into the fuel at equilibrium will be assumed to be 6% of the total (fission plus decay) linear power axial distribution values reported in the annexed specifications. Due to the quite low impact of decay heat on the short-duration beam interruptions considered, participants are free to use their own model of residual heat precursor decay.

The fuel total power variations are to be approximated by point kinetics. The constant axial power shape to be adopted with the simplified fuel element channel geometry of Table 1 is reported in Table 2. Table 2 contains linear power values (kW/m) on a regular grid (step = 3 cm) that, if needed, can be converted to the power produced within each mesh segment assuming linear variations between Table 2 couples of close data.

For any fixed axial quote, the radial power density distribution is assumed to be constant inside the fuel (but obviously zero in the central hole). The oxide-fuel axial conductivity can be neglected. An adiabatic boundary condition is assumed on the outer surface of the fuel channel.

Table 2. Linear power axial distribution

	Axial mesh boundaries (m)	Power wasted in the fuel (kW/m)
31	0.90	5.956
30	0.87	6.293
29	0.84	6.625
28	0.81	6.950
27	0.78	7.265
26	0.75	7.565
25	0.72	7.847
24	0.69	8.109
23	0.66	8.347
22	0.63	8.559
21	0.60	8.742
20	0.57	8.895
19	0.54	9.015
18	0.51	9.103
17	0.48	9.155
16	0.45	9.173
15	0.42	9.155
14	0.39	9.103
13	0.36	9.015
12	0.33	8.895
11	0.30	8.742
10	0.27	8.559
9	0.24	8.347
8	0.21	8.109
7	0.18	7.847
6	0.15	7.565
5	0.12	7.265
4	0.09	6.950
3	0.06	6.625
2	0.03	6.293
1	0.00	5.956

II. Material properties

(*T is the temperature in K.*)

Coolant conductivity (W/K∗m) [3]	$k_{Coolant} = 3.9021 + 0.0123 * T$
Coolant density (kg/m^3) [3]	$\rho_{Coolant} = 11112 - 1.375 * T$
Coolant specific heat (J/K*kg) [3]	$C_{Coolant} = 146.5$
Coolant viscosity (kg/m∗sec) [3]	$\mu_{Coolant} = 5.37 * 10^{-3} - 8.92 * 10^{-6} * T + 4.71 * 10^{-9} * T^2$
Clad conductivity (W/K*m) [3]	$k_{Clad} = 15.4767 + T * 3.448 * 10^{-3}$
Clad density (kg/m^3)	$\rho_{Clad} = 7924$
Clad specific heat (J/K*kg) [3]	$C_{Clad} = 620$
Fuel conductivity (W/K*m) [4]	$k_{Fuel} = \frac{1}{0.042 + T * 2.71 * 10^{-4}} + T^3 * 6.9 * 10^{-11}$
Fuel density (kg/m^3)	$\rho_{Fuel} = 10354$
Fuel specific heat (UO_2, PuO_2) [5] (J/K∗kg)	$C_{UO_2} = 81.825 + 0.78695 * T - 1.1552 * 10^{-3} * T^2 + 9.9037 * 10^{-7} * T^3 - 5.1982 * 10^{-10} * T^4 + 1.5241 * 10^{-13} * T^5 - 1.7906 * 10^{-17} * T^6$ $C_{PuO_2} = \frac{-4.9236 * 10^6}{T^2} + 240.89 + 0.32556 * T - 3.5398 * 10^{-4} * T^2 + 1.512 * 10^{-7} * T^3 - 1.9707 * 10^{-11} * T^4$
Fuel mixture specific heat (J/K∗kg)	$C_{Fuel} = \frac{214.65 * C_{UO_2} + 55.56 * C_{PuO_2}}{270.21}$ $\left(\frac{Weight\ PuO_2}{Weight\ (PuO_2 + UO_2)} \approx 20.5\% \right)$

III. Heat transfer correlations

1) Clad-coolant heat exchange coefficient (W/(K*m^2)) [4]:

$$h = \frac{Nu * k_{Coolant}}{D}$$

where h is the heat exchange coefficient, Nu is the Nusselt number, D is the hydraulic diameter $\left(D = \frac{4 * S}{W} \right)$, $k_{Coolant}$ is the coolant conductivity, S is the coolant flow area and W is the wetted perimeter equalling $2\pi\, r_p$.

The Nusselt number is evaluated as [4]:

$$Nu = 4 + 0.16\left(\frac{p}{2r_p}\right)^5 + 0.33\left(\frac{p}{2r_p}\right)^{3.8}\left(\frac{Pe}{100}\right)^{0.86}$$

where Pe is the Peclet number $\left(Pe = \frac{\rho_{Coolant} * V * D * C_p}{k_{Coolant}} \right)$, $\rho_{Coolant}$ is the coolant density, V is the coolant velocity, C_p is the coolant specific heat, p is the pin pitch and r_p is the outer clad radius.

2) Fuel-clad (W/(K$*$m^2)):

It is assumed that the fuel-clad gap is opened and filled with helium. Under these conditions the (approximated) heat exchange coefficient is [6]:

$$h_{gap} = \frac{3.623 * 10^{-3} * T_{gap}^{0.66}}{R_{gap}}$$

where T_{gap} is the gap filling gas temperature $\frac{T_{ex\_fuel} + T_{in\_clad}}{2}$ (T_{ex_fuel} is the outer fuel temperature and T_{in_clad} is the inner clad temperature) and R_{gap} is the gap size.

IV. Point kinetics

The effective delayed neutron fraction is assumed to be equal to 350 pcm. At full power, the system is assumed to be 8 $ sub critical (i.e. the effective multiplication factor K_{eff} = 0.97276).

The average neutron generation time, $\Lambda = 4.2 \times 10^{-7}$ s

Table 1. Delayed neutron emission group data

Group, i	Fraction, β_i	Decay constant, λ_i s^{-1}
1	8.6×10^{-5}	0.0129
2	7.30×10^{-4}	0.0313
3	6.55×10^{-4}	0.1346
4	1.267×10^{-3}	0.3443
5	5.80×10^{-4}	1.3764
6	1.82×10^{-4}	3.7425
Total	350×10^{-5}	

A. A non-linear fuel temperature feedback (reactivity) effect is assumed:

$$Reactivity_{Fuel\_feedback}(t) = \left[\overline{T}_{Fuel}(t) - \overline{T}_{Fuel}(0)\right]\frac{A_D}{\overline{T}_{Fuel}(t)}$$

where A_D is a constant coefficient A_D = -700 pcm (-2 $) and $\overline{T}_{Fuel}$ a fuel effective temperature.[5]

B. A linear coolant density feedback (reactivity) effect is assumed:

$$Reactivity_{Coolant\_feedback}(t) = \left[\overline{T}_{Coolant}(t) - \overline{T}_{Coolant}(0)\right]B_V$$

where B_V is a constant coefficient B_V = -1.2 pcm/K (-3.43 × 10^{-3} $/K) and $\overline{T}_{Coolant}$ a coolant effective temperature obtained weighting linearly (on the axial mesh size only) the different quote $\overline{T}_{Coolant}(z)$ values.

[5] $\overline{T}_{Fuel}$ can be simply calculated weighting linearly (on the axial mesh size only) the following different quote $T_{Fuel}(z)$ effective-value approximation: $\overline{T}_{Fuel}(z) = 0.3 * T_{Fuel\_Centre}(z) + 0.7 * T_{Fuel\_Boundary}(z)$.

REFERENCES

[1] D'Angelo, A., G. Bianchini, M. Carta, P. Bosio, P. Ravetto, M.M. Rostagno, "A Simple Model to Evaluate the Natural Convection Impact on the Core Transients In Liquid-metal-cooled Ads", *Proc. of the 6th OECD/NEA Information Exchange Meeting on Actinide and Fission Product Partitioning and Transmutation*, Madrid (Spain), 11-13 December 2000.

[2] Bianchini, G., M. Carta, A. D'Angelo, F. Norelli, *New Mathematical Models Implemented in the Tieste-Minosse Code*, ENEA Technical Note, SIEC/DT-SDA-00023 (2000).

[3] Cevolani, S., *Review of the Liquid Lead-bismuth Alloy Physical Properties*, ENEA Technical Note, SIEC/DT.SBD.00004, April-21-1998.

[4] Monti, S., *Thermal-hydraulic Design of the Fuel Element of the Energy Amplifier Prototype*, Cagliari 6 August 1998, ENEA Technical Note SIEC/DT-SDA-00015 November-26-1998, same title, Cagliari 6 August 1998, V. Bellucci, S. Buono, G. Fotia, L. Maciocco, V. Moreau, M. Mulas, G. Siddi, L. Sorrentino, CRS4 Technical Report, TECH-REP-98/37.

[5] Vanier, M., private communication, October 1999.

[6] Waltar, A.E., A.B. Reynolds, *Fast Breeder Reactors*, Pergamon Press (1981).

[7] D'Angelo, A., G. Bianchini, M. Carta, *Benchmark on Beam Interruptions in a Lead-bismuth-cooled and MOX-fuelled Accelerator-driven System – Specification*, OECD Nuclear Energy Agency/Nuclear Science Committee/International Working Party on Scientific Issues in Partitioning and Transmutation, NEA/SEN/NSC/WPPT(2002)6 – For Official Use.

[8] Nava, E., K.W. Burn, *Monte Carlo Calculation of the Power Distribution in the ADS-DF at BOC and EOC*, ENEA Technical Note, SIEC/DT-SBD-00021-2nd revision (2001).

Annex II

MYRRHA-TYPE SIMPLIFIED MODEL FOR FRESH FUEL CONDITIONS (CASE C & D)

B. Arien, V. Sobolev, G. Van den Eynde

Restriction: *the data in this annex are to be used by the benchmark participants only for this benchmark calculation and cannot be distributed to third parties. The data should not be used for design calculations. SCK•CEN takes no liability whatsoever concerning the correctness of the data or the use thereof.*

I. Fuel channel geometry and power data

Table 1 gives the fuel rod channel parameters for the MYRRHA experimental ADS. Bear in mind that the fuel height is 60 cm (in comparison to 90 cm in the XADS specifications) when producing results at the top (60 cm) and the mid-plane (30 cm) of the fuel zone.

In accordance with Annex I, a decay heat of 6% of the total linear power will be assumed at the equilibrium state.

Tables 2 and 3 give the axial profile of the linear power of, respectively, a hot fuel pin and an average fuel pin. If needed, linear interpolation can be used to calculate values not in the list.

The fuel total power variations are to be approximated by point kinetics.

Table 1. Fuel rod channel parameters [7]

Sizes are given at room temperature

Fuel column height	m	0.6
Pellet hole diameter	m	1.8×10^{-3}
Pellet diameter	m	7.14×10^{-3}
Clad inner diameter	m	7.37×10^{-3}
Clad outer diameter	m	8.50×10^{-3}
Fuel assembly type		Hexagonal
Pitch (“centre-to-centre” distance between the neighbour rods)	m	0.01
Coolant flow area per rod (without wire spacer)	m^2	2.986×10^{-5}
Fuel rod nominal power (“the hottest” fuel rod")	W	18 993
Coolant input temperature	K	473
Coolant outlet temperature (“the hottest” fuel rod at nominal power and flow rate)	K	~ 670

Table 2. Axial distribution of the linear power in the "hottest" fuel rod [8]

No. (from below)	Mesh boundaries (m)		Liner power in the mesh (kW/m)
	Lower	Upper	
30	0.58	0.60	14.853
29	0.56	0.58	18.111
28	0.54	0.56	20.981
27	0.52	0.54	23.618
26	0.50	0.52	26.123
25	0.48	0.50	28.548
24	0.46	0.48	30.905
23	0.44	0.46	33.180
22	0.42	0.44	35.337
21	0.40	0.42	37.330
20	0.38	0.40	39.103
19	0.36	0.38	40.603
18	0.34	0.36	41.780
17	0.32	0.34	42.591
16	0.30	0.32	43.007
15	0.28	0.30	43.009
14	0.26	0.28	42.596
13	0.24	0.26	41.779
12	0.22	0.24	40.584
11	0.20	0.22	39.050
10	0.18	0.20	37.226
9	0.16	0.18	35.167
8	0.14	0.16	32.933
7	0.12	0.14	30.578
6	0.10	0.12	28.151
5	0.08	0.10	25.683
4	0.06	0.08	23.184
3	0.04	0.06	20.631
2	0.02	0.04	17.958
1	0.00	0.02	15.050

Table 3. Axial distribution of the linear power in the "average" fuel rod [8]

No. (from below)	Mesh boundaries (m)		Liner power in the mesh (kW/m)
	Lower	Upper	
30	0.58	0.60	14.113
29	0.56	0.58	15.473
28	0.54	0.56	16.839
27	0.52	0.54	18.201
26	0.50	0.52	19.544
25	0.48	0.50	20.848
24	0.46	0.48	22.092
23	0.44	0.46	23.252
22	0.42	0.44	24.307
21	0.40	0.42	25.236
20	0.38	0.40	26.022
19	0.36	0.38	26.649
18	0.34	0.36	27.107
17	0.32	0.34	27.388
16	0.30	0.32	27.490
15	0.28	0.30	27.414
14	0.26	0.28	27.167
13	0.24	0.26	26.757
12	0.22	0.24	26.197
11	0.20	0.22	25.504
10	0.18	0.20	24.693
9	0.16	0.18	23.782
8	0.14	0.16	22.789
7	0.12	0.14	21.729
6	0.10	0.12	20.613
5	0.08	0.10	19.448
4	0.06	0.08	18.232
3	0.04	0.06	16.957
2	0.02	0.04	15.599
1	0.00	0.02	14.122

II. Materials and coolant properties – MYRRHA ADS

(*Compilation from different sources by V. Sobolev, SCK•CEN, May 2003.*)

1. Pb-Bi coolant properties (p ≈ 0.1 MPa)

Melting temperature (K)	T_{melt} = 396.65	[1]
Density(kg/m^3)	$\rho(T) = 11102 - 1.321 \cdot T$	[2]
Specific heat (J/(kg·K))	$c_p(T) = 164.0 - 4.06 \cdot 10^{-2} \cdot T + 1.33 \cdot 10^{-5} \cdot T^2$	[2]
Dynamic viscosity (Pa·s)	$\eta(T) = 4.94 \cdot 10^{-4} \cdot \exp(754.1/T)$	[2]
Thermal conductivity (W/(m·K))	$\lambda(T) = 3.35 + 1.59 \cdot 10^{-2} \cdot T - 1.95 \cdot 10^{-6} \cdot T^2$	[2]

2. T91 cladding properties

Linear thermal expansion (strain)	$\varepsilon_{LT91}(T) \equiv \left(\frac{\Delta L(T)}{L_0}\right)_{T91} = -3.0942 \cdot 10^{-3} + 1.1928 \cdot 10^{-5} \cdot T - 6.7979 \cdot 10^{-9} \cdot T^2 + 7.9606 \cdot 10^{-12} \cdot T^3 - 2.546 \cdot 10^{-15} \cdot T^4$	[3]*
Density(kg/m^3)	$\rho(T) = 7785 \cdot (1 - 3 \cdot \varepsilon_{LT91})$	[3]*
Specific heat (J/(kg·K))	$c_p(T) = 432.8 + 0.7038 \cdot T - 2.2113 \cdot 10^{-3} \cdot T^2 + 5.316 \cdot 10^{-6} \cdot T^3 - 3.105 \cdot 10^{-9} \cdot T^4$	[3]
Thermal conductivity (W/(m·K))	$\lambda(T) = 21.712 + 0.011 \cdot T - 9.5483 \cdot 10^{-6} \cdot T^2 + 3.627 \cdot 10^{-9} \cdot T^3$	[3]

** Obtained with the correlation proposed for the linear thermal expansion coefficient of $^{9\text{-}12}$Cr FMS presented in [3].*

3. *"Fresh" (non-irradiated) fuel properties – (U,Pu)O_2 MOX*

Linear thermal expansion (strain)	$\varepsilon_{L\ MOX}(T) = x \cdot \varepsilon_{L\ PuO_2}(T) + (1-x) \cdot \varepsilon_{L\ UO_2}(T)$ $\varepsilon_{L\ PuO_2}(T) \equiv \left(\frac{\Delta L(T)}{L_0}\right)_{PuO_2} = -2.7 \cdot 10^{-3} + 0.9 \cdot 10^{-5} \cdot T + 7 \cdot 10^{-2} \cdot \exp(5072/T)$ $\varepsilon_{L\ UO_2}(T) \equiv \left(\frac{\Delta L(T)}{L_0}\right)_{UO_2} = -3 \cdot 10^{-3} + 1 \cdot 10^{-5} \cdot T + 4 \cdot 10^{-2} \cdot \exp(5000/T)$	[4]
Density(kg/m^3)	$\rho_{MOX}(T) = \rho_{0\ MOX} \cdot (1 - 3 \cdot \varepsilon_{L\ MOX}(T))$ $\rho_{0\ MOX} = (1-P) \cdot (11480 \cdot x + 10960 \cdot (1-x))$	[4,5]
Specific heat (J/(kg·K))	$c_{p\ MOX}(T) = x \cdot c_{p\ PuO_2}(T) + (1-x) \cdot c_{p\ UO_2}(T)$ $c_{p\ PuO_2}(T) = \frac{1.1327 \cdot 10^8 \cdot \exp(571/T)}{T^2 \cdot [\exp(571/T) - 1]^2} + 3.95 \cdot 10^{-4} \cdot T + 4.566 \cdot 10^{11} \cdot \frac{y \cdot \exp(-23658/T)}{T^2}$ $c_{p\ UO_2}(T) = \frac{8.5013 \cdot 10^7 \cdot \exp(535.285/T)}{T^2 \cdot [\exp(535.285/T) - 1]^2} + 2.43 \cdot 10^{-2} \cdot T + 8.2935 \cdot 10^{11} \cdot \frac{y \cdot \exp(-18967/T)}{T^2}$	[4]
Thermal conductivity (W/(m·K))	$\lambda_{MOX}(T, p) = \lambda_{TD\ MOX}(T) \cdot K(P)$ $\lambda_{TD\ MOX}(T) = \frac{1.147}{0.044819 + 4 \cdot (2-y) + 2.4544 \cdot 10^{-4} (1 + 0.8 \cdot x) \cdot T} + \frac{6.327 \cdot 10^9 \cdot \exp(-16348/T)}{T^2}$	[6]

P – volumetric fraction of porosity
x – weight fraction of PuO_2
y – stoichiometry index (ratio of a number of oxygen atoms; to a number of heavy metal atoms

At the present stage of the pre-design of the MYRRHA experimental ADS the following values are used:

$$P = 0.05,\ x = 0.2995,\ y = 2.00$$

III. Heat transfer correlations

1. *Correlation for heat transfer from the cladding to LBE (triangular bundle)* [9]

$$Nu = \left(0.0165 + 0.02 \cdot \left(1 - 0.91 \cdot \left(\frac{d_{rod}}{l_{pitch}} \right)^2 \right) \cdot \left(\frac{l_{pitch}}{d_{rod}} \right)^{0.15} \right) \cdot \mathrm{Re}^{0.8} \cdot \mathrm{Pr}^{0.4}$$

where d_{rod} is the fuel rod diameter and l_{pitch} is the pitch ("centre-to-centre" distance between the neighbour rods).

2. *Correlation for heat transfer from the fuel pellet to the cladding through an open gap filled with helium ("fresh" fuel)*

$$h_{gap}(T,z) = \frac{\lambda_{He}(T)}{\delta_{gap}(T,z)}$$

if the obtained values are lower than 10 000 $\mathrm{Wm^{-2}K^{-1}}$ and:

$$h_{gap}(T,z) = 10000 \ \ Wm^{-2}K^{-1}$$

if the above formula yields values higher than 10000 $\mathrm{Wm^{-2}K^{-1}}$.

Where:

$$\lambda_{He}(T) = 2.682 \cdot 10^{-3} \left(1 + 1.123 \cdot 10^{-8} \cdot p\right) \cdot T^{0.71 \cdot \left(1 - 2 \cdot 10^{-9} \cdot p\right)}$$

is the helium thermal conductivity [10] ($\mathrm{Wm^{-1}K^{-1}}$):

$$\delta_{gap}(T,z) = \left(R_{inner\ clad\ 0} - R_{fuel\ 0}\right) \cdot \left(1 - \frac{R_{fuel\ 0} \cdot \varepsilon_{L\ MOX}\left(\overline{T}_{fuel}(z)\right) - R_{inner\ clad\ 0} \cdot \varepsilon_{L\ T91}\left(\overline{T}_{clad}(z)\right)}{R_{inner\ clad\ 0} - R_{fuel\ 0}} \right)$$

is the "pellet-cladding" radial gap (m); this formula is only valid for an open gap, where $R_{inner\ clad\ 0}$ is the inner radius of the cladding at 293.15 K (m), $R_{fuel\ 0}$ is the radius of a fuel pellet at 293.15 K (m), $\overline{T}_{fuel}(z)$ is the fuel mean actual temperature at level z (K), $\overline{T}_{clad}(z)$ is the cladding mean actual temperature at level z (K) and p is the helium pressure in the gap (Pa) (initial value at room conditions: 0.5 MPa).

IV. Point kinetics

In order to keep the results of the benchmark comparable between cases A, B (XADS) and C, D (MYRRHA), we decided to use the same level of subcriticality as in Annex I, i.e. 8$ where 1$ = 350 pcm (k_{eff} = 0.97276). It should be clearly understood that MYRRHA is not foreseen to operate at this k_{eff} (real MYRRHA k_{eff} = 0.95). The average neutron generation time and the delayed neutron group data are taken from Annex I. For the sake of completeness, the delayed neutron data is provided once again in Table 4. Only the fuel and coolant feedback correlations have been adjusted to the MYRRHA fuel.

Average neutron generation time: $\Lambda = 4.2 \times 10^{-7}$ s.

Table 4. Delayed neutron emission group data

Group, i	Fraction, β_i	Decay constant, λ_i s^{-1}
1	8.6×10^{-5}	0.0129
2	7.30×10^{-4}	0.0313
3	6.55×10^{-4}	0.1346
4	1.267×10^{-3}	0.3443
5	5.80×10^{-4}	1.3764
6	1.82×10^{-4}	3.7425
Total	350×10^{-5}	

Fuel temperature feedback correlation

$$\Delta\rho_{fuel}(t) = f \cdot \left[1 - \left(\frac{\overline{T}_F(0)}{\overline{T}_F(t)} \right)^{0.1} \right]$$

where f = -2 500 pcm and $\overline{T}_F(t)$ is a fuel effective temperature which can be calculated as the axial average of $\overline{T}_F(z) = 0.3 * T_F(centreline) + 0.7 * T_F(boundary)$.

Coolant temperature feedback correlation

$$\Delta\rho_{cool}(t) = a \cdot \left(\overline{T}_C(t) - \overline{T}_C(0)\right)^2 + b \cdot \left(\overline{T}_C(t) - \overline{T}_C(0)\right)$$

where a = 0.005 pcm/K^2 and b = -1.823 pcm/K. $\overline{T}_C(t)$ is a coolant effective temperature calculated as the axial average of $\overline{T}_C(z)$ values.

REFERENCES

[1] Kutateladze, S.S., *et al*., "Liquid Metal Heat Transfer Media", translated from Russian, Suppl. No. 2 of the *Soviet Journal of Atomic Energy* (1958). Consultants Bureau, Inc., New York, Chapman & Hall, Ltd. London (1959), 149 p.

[2] Sobolev, V. *Database of Thermal Properties for the Melted Lead-bismuth Eutectic*, Internal Report: IR-18. SCK•CEN, Mol, Belgium, May 2002.

[3] Dai, Y., *Preliminary Database of T91*, communication of 8 May 2000.

[4] *SCDAP/RELAP/MOD3.1 Code Manual; Vol. IV: MATPRO – A Library of Materials Properties for Light-water-reactor Accident Analysis*, D.T. Hagrman (ed.), INEL Report NUREG/ CR-6150, Idaho, USA (1993).

[5] Wirtz, K., *Lectures on Fast Reactors*, Kernforschungszentrum und Universität Karlsruhe, Karlsruhe, Postfach 3640, 7500 Karlsruhe, Germany (1978).

[6] Baron, D., "About the Modelling of Fuel Thermal Conductivity Degradation at High Burn-up Accounting for Recovering Process with Temperature", *Proc. of the Seminar on Thermal Performance of High Burn-up LWR Fuel*, Cadarache, France, 3-6 March 1998.

[7] Sobolev, V., *Reference Fuel Assembly Design for the Sub-critical Core of ADS MYRRHA*, Technical Note NT-32-B043-0133, Reactor Physics & MYRRHA Department, SCK•CEN, Mol, Belgium, September 2001.

[8] Malambu, E.M., Th. Aoust, N. Messaoudi, G. Van den Eynde and Ch. De Raedt, *Status of Neutronics Analysis of the MYRRHA ADS: Progress Report on November 2001*, Report R-3593, SCK•CEN, Mol, Belgium, March 2002.

[9] Kirillov P.L., Yu.S. Yuriev, V.P. Bobkov, *Handbook: Thermohydraulic Calculations (Nuclear Reactors, Heat Exchangers, Steam Generators)*, Moscow: Energoizdat (1990) (in Russian).

[10] Petersen, H., *The Properties of Helium – Density, Specific Heat, Viscosity and Thermal Conductivity at Pressures from 1 to 100 bar and from Room Temperature to 1 800 K*, Risø Report, No. 224, September 1970.

Appendix II

THE POROSITY CORRECTION FOR MOX THERMAL CONDUCTIVITY

The porosity correction for MOX thermal conductivity of MYRRHA experimental ADS cases ("C" and "D") was not typed in the document NEA/SEN/NSC/WPPT(2003)7: *Beam Interruptions in a Lead-bismuth-cooled and MOX-fuelled Accelerator-driven System. Benchmark Specification: Phase II*.

The Porosity Correction K(P) for MOX Thermal conductivity of MYRRHA experimental ADS cases ("C" and "D") is:

$$K(P) = 1 - \left(2.7384 - 5.8 \cdot 10^{-4} \cdot T\right) \cdot P$$

The corresponding thermal conductivity complete formulation is:

Thermal conductivity	$W/(m \cdot K)$	$\lambda_{MOX}(T,p) = \lambda_{TD\ MOX}(T) \cdot K(P)$ $\lambda_{TD\ MOX}(T) = \dfrac{1.147}{0.044819 + 4 \cdot (2-y) + 2.4544 \cdot 10^{-4}(1 + 0.8 \cdot x) \cdot T} + \dfrac{6.327 \cdot 10^{9} \cdot \exp(-16348/T)}{T^{2}}$ $K(P) = 1 - \left(2.7384 - 5.8 \cdot 10^{-4} \cdot T\right) \cdot P$	[6]

where P is the volumetric fraction of porosity, x is the weight fraction of PuO_2 and y is the ratio of a number of oxygen atoms to a number of heavy metal atoms.

At the present stage of the pre-design of the MYRRHA experimental ADS the following values are used:

$$\boxed{P = 0.05,\ x = 0.2995,\ y = 2.00}$$

OECD PUBLICATIONS, 2 rue André-Pascal, 75775 PARIS CEDEX 16
Printed in France.